



Cite this: *Chem. Soc. Rev.*, 2025, **54**, 3906

## Body fluid diagnostics using activatable optical probes

Jie Zhan, <sup>a</sup> Yanbin Cai, <sup>b</sup> Penghui Cheng,<sup>\*c</sup> Lei Zheng <sup>\*a</sup> and Kanyi Pu <sup>\*de</sup>

*In vitro* diagnostics often detects biomarkers in body fluids (such as blood, urine, sputum, and cerebrospinal fluids) to identify life-threatening diseases at an early stage, monitor overall health, or provide information to help cure, treat, or prevent diseases. Most clinically used optical *in vitro* diagnostic tests utilize dye-labeled biomolecules for biomarker recognition and signal readout, which typically involve complex steps and long processing times. Activatable optical probes (AOPs), which spontaneously activate their optical signals only in the presence of disease biomarkers, offer higher signal-to-background ratios and improved detection specificity. They also have the potential to simplify detection procedures by eliminating multiple washing steps. In this review, we summarize recent advances in the use of AOPs for pre-clinical and clinical body fluid diagnostics across various diseases, including cancer, nephro-urological disorders, infectious diseases, and digestive diseases. We begin by discussing the molecular design strategies of AOPs to achieve different optical signal readouts and biomarker specificity. We then highlight their diagnostic applications in various disease models and body fluids. Finally, we address the challenges and future perspectives of AOPs in enhancing body fluid diagnostics and advancing precision medicine.

Received 26th December 2024

DOI: 10.1039/d4cs01315h

[rsc.li/chem-soc-rev](https://rsc.li/chem-soc-rev)

<sup>a</sup> Department of Laboratory Medicine, Guangdong Provincial Key Laboratory of Precision Medical Diagnostics, Guangdong Engineering and Technology Research Center for Rapid Diagnostic Biosensors, Guangdong Provincial Key Laboratory of Single Cell Technology and Application, Nanfang Hospital, Southern Medical University, Guangzhou, 510515, China. E-mail: [nfyzyhenglei@smu.edu.cn](mailto:nfyzyhenglei@smu.edu.cn)

<sup>b</sup> Guangdong Provincial Biomedical Engineering Technology Research Center for Cardiovascular Disease, Department of Cardiology and Laboratory of Heart Center, Zhujiang Hospital, Southern Medical University, Guangzhou, 510280, China

<sup>c</sup> State Key Laboratory of Natural Medicines, China Pharmaceutical University, Nanjing, 211198, China. E-mail: [penghui.cheng@126.com](mailto:penghui.cheng@126.com)

<sup>d</sup> School of Chemistry, Chemical Engineering and Biotechnology, Nanyang Technological University, 70 Nanyang Drive, Singapore, 637457, Singapore. E-mail: [kypu@ntu.edu.sg](mailto:kypu@ntu.edu.sg)

<sup>e</sup> Lee Kong Chian School of Medicine, Nanyang Technological University, 59 Nanyang Drive, 636921, Singapore, Singapore



**Jie Zhan**

Jie Zhan obtained her PhD degree in Biochemistry and Molecular Biology from Nankai University in 2019. She joined the Nanfang Hospital of Southern Medical University as an associate professor in 2022. She is currently a visiting scholar at Nanyang Technological University. Her research focuses on the application of self-assembled peptides and molecular probes for *in vitro* diagnostics and therapy in cardiovascular diseases and cancer.



**Yanbin Cai**

Yanbin Cai obtained his PhD degree in 2017 from Nankai University under the supervision of Professor Zhimou Yang. He then joined the Zhujiang Hospital of Southern Medical University as an associate professor and was promoted to full professor in 2023. His research interests focus on peptide molecular self-assembly and functional materials for applications in drug delivery, theranostics, and biomimetic systems.



# 1. Introduction

*In vitro* diagnostics (IVD) refers to the analytical technologies used to examine the pathophysiological state of biological specimens from living organisms under extracorporeal conditions, and has become an integral part of modern healthcare in disease diagnostics, health monitoring, and instructed clinical decision.<sup>1</sup> IVD involves a wide range of sample types, including body fluids, secretions/excretions, tissues, and cells. As compared to other types of IVD, body fluid (blood, urine, sputum, tears, saliva, *etc.*)-based diagnostics offers advantages such as directly reflecting the pathological states of various organs, minimally invasive sampling procedures, and high reproducibility.<sup>2</sup> Therefore, body fluid diagnostics has remained as the most prevalent and widely applied form of IVD. Current clinical approaches of body fluid diagnostics encompass a variety of methods, including immunological methods (enzyme-linked immunosorbent assay (ELISA), chemiluminescence immunoassay (CLIA), flow cytometry, *etc.*), molecular diagnostic methods (polymerase chain reaction (PCR) and

variants of reverse transcription-polymerase chain reaction (RT-PCR), and quantitative real-time polymerase chain reaction (qPCR)), clinical chemistry methods (spectrophotometry, electrochemistry, and colorimetry), hematology methods (complete blood count and coagulation tests), microbiology methods (culture and sensitivity testing and mass spectrometry), *etc.*<sup>3</sup>

In order to improve detection sensitivity and spatial resolution, optical IVD approaches utilizing dye-labeled biomolecules for biomarker recognition and signal readout have been developed, such as colorimetry, CLIA, fluorescence immunoassay, qPCR, *etc.* However, these methods are typically time-consuming, labor-intensive, and require specialized personnel and instrumentation.<sup>4</sup> For example, conventional immunoassays typically require 4+ hours of processing time (from sample collection to result reporting) with 5+ steps, including sample preparation, incubation, multiple washing, signal detection and result interpretation. These steps are crucial to reduce background signals and enhance signal-to-background ratios (SBRs), and any deviations can lead to false positive or false negative results.<sup>5</sup> While automation has significantly improved operational efficiency and reduced human errors in clinical laboratories, the assay's inherent complexity continues to pose challenges, such as variations in sample handling and instrument calibration.<sup>6</sup> These limitations underscore the importance of developing more simplified and advanced diagnostic approaches to maintain high accuracy.

Activatable optical probes (AOPs) are a class of optical agents that spontaneously activate their optical signals in the presence of disease biomarkers, thereby offering high SBRs and improved detection sensitivity and specificity.<sup>7–9</sup> To date, a variety of AOPs have been applied in body fluid diagnostics.<sup>10,11</sup> As compared to clinical assays, these AOP-based body fluid diagnostics have substantially simplified protocols: they only require direct addition of AOPs into (pre)clinical specimens, followed by a short incubation time and subsequent optical signal readout. This streamlined process not only reduces procedural complexity



**Penghui Cheng**

*Penghui Cheng received her PhD degree from Nanyang Technological University in 2022 under the supervision of Prof. Kanyi Pu. After postdoctoral studies with Prof. Kanyi Pu, she joined China Pharmaceutical University, State Key Laboratory of Natural Medicines, Center of Drug Discovery in 2024 as a full Professor. Her current research interests include the development of smart imaging probes for disease theranostics and new drug development.*



**Lei Zheng**

*Lei Zheng is a professor at the Nanfang Hospital of Southern Medical University. He serves as the Editor-in-Chief of Interdisciplinary Medicine and Associate Editor of Journal of Extracellular Vesicles. His research interests focus on the development and clinical translation of novel in vitro diagnostic technologies, as well as the study and application of extracellular vesicles.*



**Kanyi Pu**

*Kanyi Pu is a President's Chair Professor at Nanyang Technological University (NTU), where he is affiliated with both the School of Chemistry, Chemical Engineering and Biotechnology and the Lee Kong Chian School of Medicine. He is the Executive Editor of the Journal of the American Chemical Society and serves on the editorial advisory boards of over 18 prestigious journals, including Chemical Society Reviews, Advanced Functional Materials, and Biomaterials.*

*His research is focused on molecular optical imaging and nanomedicine, and he is particularly recognized for his groundbreaking work in molecular afterglow imaging and the development of artificial urinary biomarker probes.*



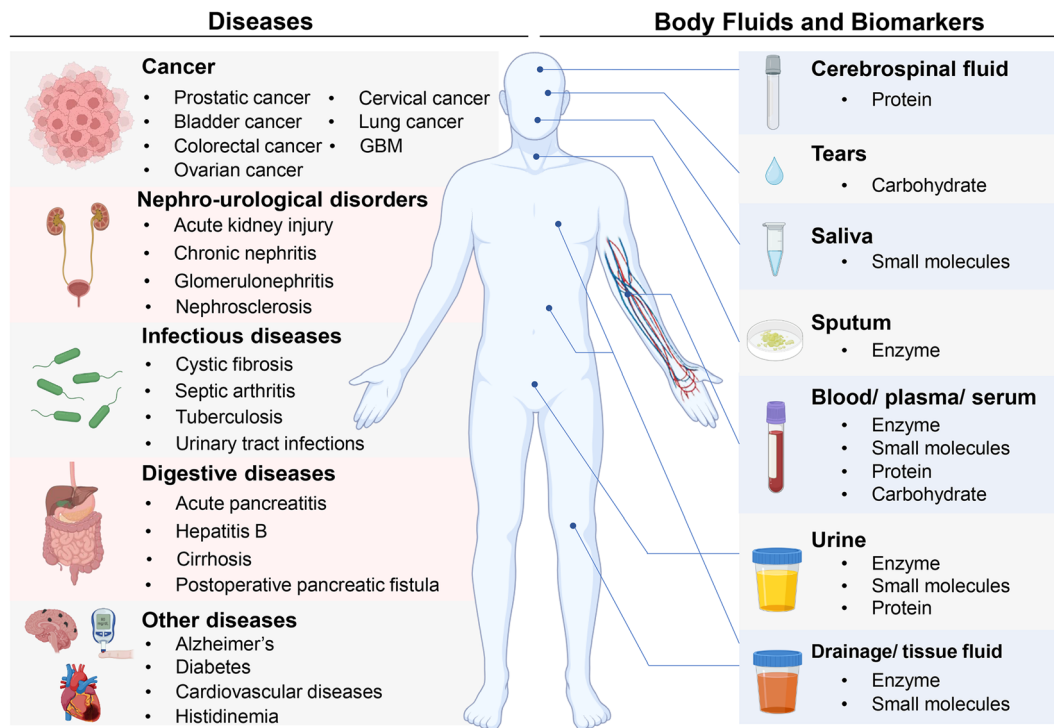


Fig. 1 Body fluid-based disease diagnostics. An overview of diseases, body fluids, and biomarkers relevant to AOP applications in *in vitro* diagnostics. Created in Biorender.com.

by eliminating repetitive washing steps and reducing sample manipulation, but also potentially improves diagnostic performance and achieves disease detection at an incipient stage. Moreover, by integrating molecular recognition and signal transduction into a single entity, AOP-based body fluid diagnostics could be developed into point-of-care testing (POCT) devices. This integration represents a significant advancement towards more efficient, rapid, and accessible *in vitro* diagnostic tools, making them particularly valuable across various clinical applications, especially in resource-limited settings or when rapid results are crucial.<sup>12,13</sup>

In this review, we summarize recent advances in AOP-based body fluid diagnostics under various pathological conditions (cancer, nephro-urological disorders, infectious diseases, digestive diseases, *etc.*) (Fig. 1 and Table 1). The molecular design strategies of AOPs that enable diverse optical signal readouts and biomarker specificity are first discussed. The diagnostic utility of these AOPs is then elaborated in various disease models and body fluids. Finally, the challenges and future perspectives related to improving body fluid diagnostics and advancing the field of precision medicine are explored.

## 2. Molecular designs

To perform body fluid-based disease diagnostics, effective AOP designs meet the following two requirements. First, the AOP should be developed based on common optical imaging agents (molecular fluorophores,<sup>9,49</sup> quantum dots,<sup>50</sup> multifunctional nanomaterials,<sup>51</sup> *etc.*) and exhibits an obvious spectra change

upon biomarker detection. To enhance SBRs and improve spatial resolution, AOPs with a “turn-on” signal response have been reported. Ratiometric AOPs with shifts in emission profiles have also been developed for biomarker quantification. Second, AOPs should demonstrate sensitive and specific detection capabilities towards biomarker-of-interest. Suitable sensing mechanisms could be incorporated into AOP molecular designs to achieve chemoselectivity towards various biomarkers in body fluids, such as enzymes,<sup>52,53</sup> small molecules,<sup>52,54</sup> proteins,<sup>55</sup> *etc.*

AOPs could be classified into different categories based on their molecular design strategies, such as charge transfer processes,<sup>56</sup> energy transfer processes,<sup>50</sup> photoinduced electron transfer (PET)<sup>57</sup> and aggregation-induced emission (AIE)<sup>58</sup> (Fig. 2). For example, several AOPs with signals “turn-ON” are designed based on charge transfer processes, including intramolecular charge transfer (ICT) and twisted intramolecular charge transfer (TICT). For ICT-based AOPs (1, 5, and 11), they are designed based on fine-tuning of the charge transfer processes, where the incorporation of biomarker-responsive moieties on optical-tunable atoms disrupts the charge transfer processes, and ICT processes are recovered with fluorescence enhancement upon biomarker recognition (Fig. 2a). In addition, several TICT-based AOPs (17, 19, and 20) have been developed for albumin detection, where the initial intramolecular rotation enables charge separation (TICT ON), and upon albumin binding, the intramolecular rotation becomes restricted in the protein hydrophobic cavity (TICT OFF), resulting in fluorescence activation (Fig. 2b).

Based on energy transfer processes (for example, Förster resonance energy transfer/FRET), several AOPs (33 and 39)



Table 1 Summary of AOPs for body fluid diagnostics of diseases

Body fluid	Biomarker-AOP of-interest	Design mechanism	Detection type	Signal output $\lambda_{ex}/\lambda_{em}$ (nm)	Detection range	LOD	Measurement time	Body fluid volume	Ref.
<b>Cancer detection</b>									
Blood plasma	1 GGT	ICT	Blue shift	Before: 730/805 After: 540/640	0.1–90.0 U L <sup>-1</sup>	0.03 U L <sup>-1</sup>	16 min	NR	14
Blood serum	2 GGT	ICT	Turn on	$\lambda_{em}$ : 571	0–20 U L <sup>-1</sup>	0.66 mU L <sup>-1</sup>	30 min	NR	15
Blood plasma	3 Hcy	ICT	Turn on	488/550	0.625–160 $\mu$ M	0.176 ppm	5 min	NR	16
Whole blood	4 H <sub>2</sub> O <sub>2</sub>	ICT	Turn on	One-photon: 400/450 Two-photon: 800/450	0–100 $\mu$ M	0.1 $\mu$ M	NR	NR	17
Urine	5 APN	ICT	Turn on	695/720	NR	NR	7 days post tumor implantation	NR	18
Urine	6 Cys	ICT	Turn on	488/550	0–10 ng $\mu$ L <sup>-1</sup>	1 ng mL <sup>-1</sup>	40 min	200 $\mu$ L	19
Urine	7 Cys, Hcy	ICT	Turn on	480/630(Cys) 480/560(Hcy)	80–1280 $\mu$ M (Cys and Hcy)	0.64 $\mu$ M (Cys) 3.2 $\mu$ M (Hcy)	Cys: $V_{1/2}$ = 26.6 min Hcy: $V_{1/2}$ = 192.1 min	198 $\mu$ L	20
Urine	8 sLe <sup>x</sup>	PET	Turn on	255/426	NR	$4.58 \times 10^{-10}$ mol L <sup>-1</sup>	15 min	1 mL	21
Saliva	9 NO	FRET	Turn on	680/780	0–20 $\mu$ M	28 nM	5 min	NR	22
Lung fluid	10 Long-chain aldehydes	PET	Turn on	373/530	0–250 $\mu$ M (nonanal)	Nonanal: 10 $\mu$ M Heptanal: 40 $\mu$ M Octanal: 100 $\mu$ M	15 min	100 $\mu$ L	23
<b>Nephro-urological disorder detection</b>									
Urine	11 NAG	ICT	Turn on	695/720	NR	NR	30–60 min	100 $\mu$ L	24
Urine	12 GGT	ICT	Turn on	380/440	NR	NR	1 h	100 $\mu$ L	25
Urine	13 AAP	ICT	Turn on	550/590	NR	NR	1 h	100 $\mu$ L	25
Urine	14 DPP-IV	FRET	Turn on	450/520	NR	NR	1 min	NR	26
Urine	15 GGT	FRET	Turn on	450/520	NR	NR	1 min	NR	26
Urine	16 HSA	ICT	Blue shift	Before: 400/580 After: 400/490	0–200 $\mu$ g mL <sup>-1</sup>	0.2 $\mu$ g mL <sup>-1</sup>	3 min	300 $\mu$ L	27
Urine	17 HSA	TICT	Turn on	555/635	0–1.0 g L <sup>-1</sup>	0.36 mg L <sup>-1</sup>	<25 min	NR	28
Urine	18 HSA	AIE	Turn on	360/490	0.02–3000 mg L <sup>-1</sup>	0.21 nM	10 s	25 $\mu$ L	29
Urine	19 HSA	TICT	Turn on	520/590	0–0.4 mg mL <sup>-1</sup>	1.89 $\mu$ g mL <sup>-1</sup>	0.5 min	NR	30
Urine	20 mALB	AIE&TICT	Turn on	454/680	0–800 $\mu$ g mL <sup>-1</sup>	3.15 $\mu$ g mL <sup>-1</sup>	NR	NR	13
<b>Infectious diseases detection</b>									
Sputum	21 Rv3368c	PET	Turn on	561/565	NR	$3.5 \times 10^2$ CFU for <i>M. smegmatis</i> $4.3 \times 10^2$ CFU for H37Rv	2 h	2 mL	31
Sputum	22 $\beta$ -Lactamase	ICT	Turn on	490/520	NR	10 CFU	<10 min	100 $\mu$ L	12
Sputum	23 $\beta$ -Lactamase	ICT	Turn on	490/520	< $1.6 \times 10^7$ CFU mL <sup>-1</sup>	10 CFU	1 h	100 $\mu$ L	32
Sputum	24 Antigen 85	Polarity responsiveness	Turn on	$\lambda_{ex}$ = 405 nm (optimal) or 488 nm $\lambda_{em}$ = 515–535 nm	NR	10 000 CFU mL <sup>-1</sup>	30 min	100 $\mu$ L	33
Synovial fluid	25 Micrococcal nuclease	FRET	Turn on	$\lambda_{ex}$ = 480/490 nm $\lambda_{em}$ = 515–535 nm	NR	NR	2 h	1 mL	34
Synovial fluid	26 Caspase-1	NSET	Turn on	FITC/GFP filter sets	5 to 20 (average number of <i>S. aureus</i> in one host cell)	5 (average number of <i>S. aureus</i> in one host cell)	1 h	NR	35
Urine	27 ESBL/AmpC	ICT	Turn on and red shift	Before: $\lambda_{max}$ = 436 nm After: $\lambda_{max}$ = 512 nm	$5 \times 10^3$ – $5 \times 10^6$ CFU mL <sup>-1</sup>	$5 \times 10^4$ CFU mL <sup>-1</sup>	5 min	20 $\mu$ L	36





Table 1 (continued)

Body fluid	Biomarker-AOP of-interest	Design mechanism	Detection type	Signal output $\lambda_{ex}/\lambda_{em}$ (nm)	Detection range	LOD	Measurement time	Body fluid volume	Ref.
Urine	28 Carbapenemases	ICT	Turn on and red shift	Before: $\lambda_{max} = 417$ nm After: $\lambda_{max} = 591$ nm	$5 \times 10^3 - 5 \times 10^6$ CFU mL <sup>-1</sup>	$5 \times 10^4$ CFU mL <sup>-1</sup>	5 min	20 $\mu$ L	36
Digestive system disease detection									
Blood serum	29 LAP, MAO	ICT	Turn on	670/720	0–20 U L <sup>-1</sup>	NR	2 h	NR	37
Blood serum	30 LAP, MAO	ICT	Turn on	365/520	<12.5 U L <sup>-1</sup>	LAP: 0.877 U L <sup>-1</sup> MAO: 0.249 U L <sup>-1</sup>	Plateau: 24 h; strip: < 1 min	NR	38
Blood serum	31 LPS, AMY	AIE	Turn on	390/460 (LPS) 390/610 (AMY)	LPS: 0–72 U L <sup>-1</sup> AMY: 0–110 U L <sup>-1</sup>	LPS: 0.11 U L <sup>-1</sup> AMY: 0.17 U L <sup>-1</sup>	LPS: 7 min AMY: 25 min	NR	39
Blood serum	32 $\alpha$ -Amylase	AIE	Turn on	370/482	0–45.5 U L <sup>-1</sup>	0.14 U L <sup>-1</sup>	3 min	NR	40
Drainage fluid	33 Pancreatic proteases	FRET	Blue shift	Before: 490/620 After: 490/520	NR	Trypsin: 5.00 U mL <sup>-1</sup> $\alpha$ -Chymotrypsin: 0.02 U mL <sup>-1</sup> Elastase: 0.003 U mL <sup>-1</sup>	10 min	NR	41
Other disease detection									
Whole blood	34 Hydrogen sulfide (H <sub>2</sub> S)	PET	Turn on	580/680	NR	28 nM	50 min	NR	42
Blood serum	35 HClO	ICT	Turn on	620/690	5.0–45 $\mu$ M	0.29 $\mu$ M	2 s	NR	43
Blood serum and urine	36 Histidine	Ligand substitution	Turn on	400/645	$1.4 \times 10^{-5}$ to $6.5 \times 10^{-10}$ mol L <sup>-1</sup>	$3.2 \times 10^{-10}$ mol L <sup>-1</sup>	NR	Serum: 1 mL Urine: 0.1 mL	44
Blood	37 Viscosity	TBET	Ratiometric	Before: 375/460 After: 375/675	16.1–611 cp	NR	NR	10 $\mu$ L	45
Urine	38 MDA	ICT and PET	Turn on	730/760	0–500 $\mu$ M	163 nM	30 min	10 $\mu$ L	46
Tear	39 Glucose	FRET	Turn on	490/652	0.03–3 mmol L <sup>-1</sup>	NR	30 s	2 $\mu$ L	47
CSF	40 A $\beta$ ligomers	ICT	Turn on	465/577	NR	$0.57 \pm 0.04$ nM	2 h	NR	48

Abbreviations: AAP, alanine aminopeptidase; A $\beta$ , amyloid- $\beta$ ; AIE, aggregation-induced emission; AMY,  $\alpha$ -amylase; APN, aminopeptidase N; CSF, cerebrospinal fluid; Cys, cysteine; DPP-IV, dipeptidyl peptidase-IV; ESBL/AmpC, extended-spectrum/AmpC  $\beta$ -lactamases; FRET, Förster resonance energy transfer; GGT,  $\gamma$ -glutamyl transpeptidase; HClO, hypochlorous acid; Hcy, homocysteine; H<sub>2</sub>S, hydrogen sulfide; HSA, human serum albumin; ICT, intramolecular charge transfer; LAP, leucine aminopeptidase; LOD, limit-of-detection; LPS, lipase; mALB, microalbumin; MAO, monoamine oxidase; MDA, malondialdehyde; NAG, *N*-acetyl-beta-D-glucosaminidase; NO, nitric oxide; NR, not reported; NSET, nanomaterial-based surface energy transfer; PET, photoinduced electron transfer; Rv3368c, nitroreductase Rv3368c; sLe<sup>x</sup>, sialyl Lewis X; TBET, through bond energy transfer; TICT, twisted intramolecular charge transfer.

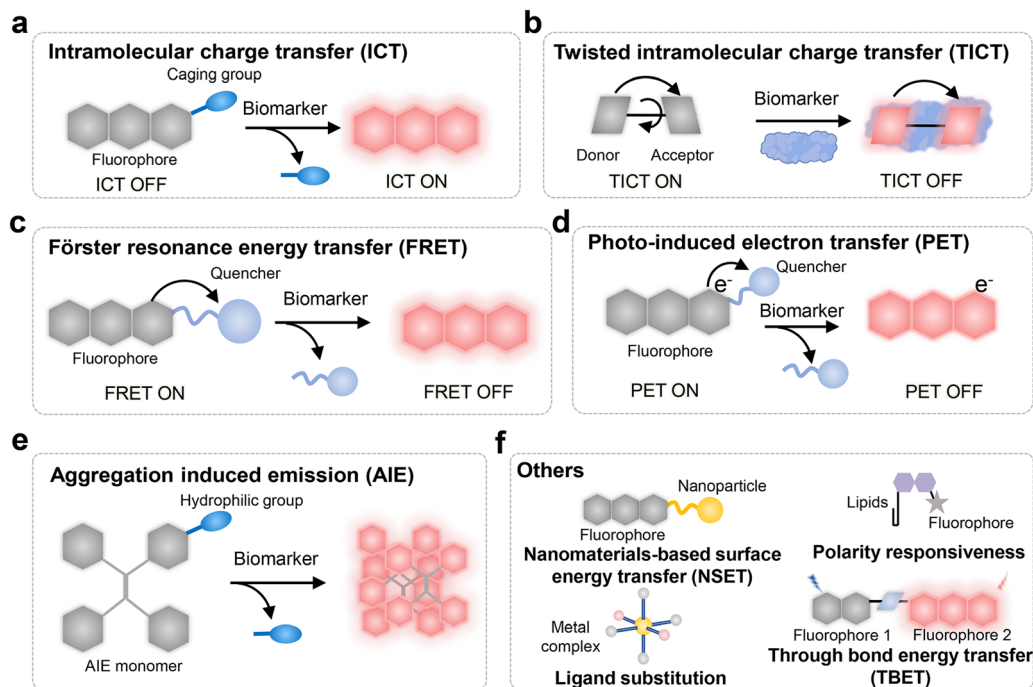


Fig. 2 AOP molecular design strategies. Schematic illustration of AOP molecular design strategies: (a) ICT, (b) TICT, (c) FRET, (d) PET, (e) AIE, and (f) others.

are designed through a facile strategy by conjugating a donor fluorophore and a quencher *via* a biomarker-cleavable linker, and biomarker cleavage results in shifts in fluorescence emission (Fig. 2c). Besides, PET-based AOP 21 has been developed by conjugating an electron-withdrawing nitrobenzyl group onto fluorophores to achieve a nitroreductase-activatable response. AOP 21 initially exhibits minimal fluorescence due to intramolecular electron transfer, and fluorescence is recovered after biomarker cleavage. AIE represents a unique mechanism where dispersed molecules show minimal emission, but biomarker-induced aggregation restricts molecular motion, leading to enhanced fluorescence emission (Fig. 2d), typically observed in tetraphenylethene derivatives that become highly fluorescent upon analyte-induced aggregation (AOPs 31, 32).

AOPs have also been developed based on other molecular design strategies, including nanomaterial-based surface energy transfer (NSET),<sup>59</sup> through bond energy transfer (TBET),<sup>60</sup> ligand substitution,<sup>61</sup> and polarity responsiveness (Fig. 2e).<sup>62</sup> NSET refers to the dipole-surface energy transfer between fluorophores and nanomaterial surfaces. For example, AOP 26 is developed by conjugating fluorescently labeled substrates onto gold nanoparticles, and fluorophores are released upon biomarker cleavage. TBET is a highly efficient energy transfer process based on a conjugated donor-acceptor system connected *via* rigid  $\pi$ -electronic bridges for rapid and efficient energy migration. Upon biomarker recognition, structural or electronic perturbations of the conjugated pathway modulate the energy transfer process, resulting in ratiometric fluorescence changes (AOP 37). Ligand substitution-based AOPs (for example, AOP 36) are molecular sensors that utilize coordination chemistry to achieve signal transduction, wherein the exchange of ligands around a metal

center induces a transition in optical properties. Polarity responsiveness-based AOPs usually modulate their emission properties based on changes in the local environmental polarity and exhibit distinct photophysical behaviors in environments of different polarities. For example, AOP 24 represents a polarity-responsive design where enzymatic incorporation and then into the hydrophobic mycomembrane triggers dramatic fluorescence enhancement through environmental polarity transition from aqueous to lipophilic conditions.

These various molecular mechanisms exhibit distinct advantages and are suitable for different detection scenarios. For instance, ICT/TICT-based mechanisms offer broad applicability and versatility in molecular design, though their performance is susceptible to environmental factors, particularly pH. FRET-based probes achieve excellent ON/OFF contrast and are particularly valuable for detecting DNA and protein, though their efficiency depends on the donor-acceptor distance and spectral overlap. PET-based designs demonstrate a rapid response and high sensitivity to electrical potential changes, making them ideal for ion detection and neurotransmitter monitoring. AIE-based probes are particularly useful for imaging in aggregation-induced analytes, such as in cellular membranes or amyloid fibrils, while their performance may be compromised in highly soluble or dispersed systems. Therefore, selecting an appropriate luminescence mechanism, or even combining multiple mechanisms, based on specific application conditions is crucial for the design and application of AOPs.<sup>63–65</sup>

### 3. Body fluid diagnostics using AOPs

AOPs have emerged as promising detection tools in body fluid diagnostics, demonstrating superior advantages over other



(pre)clinical diagnostic approaches through their rapid detection, high sensitivity, and minimal sample requirements across various pathological conditions. Therefore, AOP-based body fluid diagnostics has been successfully implemented in the diagnosis of many major diseases, including cancer, genitourinary disorders, infectious diseases, gastrointestinal diseases, neurodegenerative diseases, cardiovascular disorders, *etc.* Additionally, AOPs feature user-friendly operational protocols and straightforward signal readout methods that require minimal technical expertise, making them suitable for deployment in primary healthcare settings and home-based monitoring. The specific applications of AOP-based body fluid diagnostics in various disease categories will be elaborated in more detail in the following sections.

### 3.1. Cancer

Cancer is one of the leading causes of death globally with high morbidity and mortality.<sup>66</sup> Therefore, cancer diagnosis at an early disease stage is crucial to achieve effective treatment and improved patient outcomes. Tumor-associated biomarkers, representing a diverse array of small molecules, enzymes, and reactive species that are distributed across various body fluids (blood, urine, saliva, and tissue fluid), offer a wealth of detection targets and sample sources for tumor detection.<sup>67</sup> Though current clinical detection methods such as ELISA, MS, and PCR have been widely employed to detect tumor-associated biomarkers, these techniques often require sophisticated instrumentation, complex sample preparation procedures, and substantial analytical expertise, leading to time-consuming and costly analyses.<sup>68</sup> In contrast, AOP-based body fluid diagnostics enables short detection times, simplified sample preparation protocols, accessible operational procedures, and cost-effective implementation, while maintaining sensitivity levels comparable to standard commercial assay platforms. This innovative technology paves the way for precision oncology, promising to significantly enhance the accuracy and timeliness of cancer diagnostics.

**3.1.1. Blood.** Blood, a vital component of the human body, is the main constitution of the whole-body circulatory system and serves as the primary medium for clinical diagnosis.<sup>69</sup> With systemic circulation throughout the body, blood carries a series of substances, including cells, proteins, metabolites, *etc.* This complex mixture reflects the physiological and pathological states of various organs and tissues, making blood an invaluable source of information for diagnosing and monitoring diseases.<sup>70</sup> In the field of cancer diagnostics and monitoring, hematological analysis occupies a prominent position. Circulating components from tumor microenvironments, including small molecules, proteins and enzymes, have significant diagnostic potential as tumor-specific biomarkers.<sup>71</sup> These biomarkers provide additional evidence of cancer activity, complementing existing blood-based diagnostic methods and potentially enhancing the accuracy of cancer detection and monitoring.

$\gamma$ -Glutamyl transpeptidase (GGT) is a membrane protease associated with tumor progression, invasion, and chemoresistance, and its overexpression has been reported in various

human malignancies (ovarian, cervical, liver tumors, *etc.*).<sup>72</sup> The elevated serum GGT level is associated with an increased risk of cancer progression, invasion, and migration.<sup>73</sup> In response to the diagnostic potential of GGT, Li's and Yang's groups reported GGT-activatable fluorescent and bioluminescent AOPs **1** and **2** (Fig. 3).<sup>14,15</sup> AOP **2** was constructed by caging the D-luciferin hydroxyl group with the GGT-cleavable  $\gamma$ -glutamyl group through a self-immolative linker. The  $\gamma$ -glutamyl bond was cleaved in the presence of GGT to release active D-luciferin. Due to the absence of excitation-induced autofluorescence, AOP **2** achieved a remarkable limit of detection (LOD) value of 0.66 mU L<sup>-1</sup>. The AOP **2**-based serum test was then applied to distinguish ovarian carcinoma patients from healthy controls with clinical serum samples and achieved high accuracy (Fig. 4a). Notably, the detection results obtained with AOP **2** show complete concordance with those from commercial GGT assay kits.

The elevated serum level of homocysteine (Hcy), hyperhomocysteinemia, has been correlated with an increased risk of various cancers (such as colorectal cancer, glioblastoma, breast cancer, bladder cancer, *etc.*).<sup>74</sup> Kim's group reported a Hcy-activatable fluorescent probe (AOP **3**) for real-time monitoring of serum Hcy levels with diagnostic and prognostic purposes.<sup>16</sup> AOP **3** utilized pyridine-thiol coordination and amine-addition reaction mechanisms to achieve selective Hcy detection (Fig. 3). As shown in Fig. 4b, AOP **3** showed remarkable responsiveness to Hcy in plasma with a low LOD value (0.084 ppm) and a rapid response time (within 5 minutes). The AOP **3**-based blood test was then applied to monitor tumor progression in the glioblastoma (GBM) tumor mice model and up to ~1.6-fold elevated bioluminescence signals were observed at 7 days post-tumor implantation. In contrast, AOP **3**-based real-time imaging only detected tumor growth at 14 days post-tumor implantation. Therefore, the AOP **3**-based blood test could effectively detect GBM at an early stage (Fig. 4c). In addition to biothiols, other small molecules have also emerged as potential biomarkers for cancer diagnosis. For example, Zhu's group developed a hydrogen peroxide (H<sub>2</sub>O<sub>2</sub>)-responsive fluorescent nanoprobe (AOP **4**, Fig. 3) to assist the identification of circulating tumor cells (CTCs).<sup>17</sup> AOP **4** consists of a H<sub>2</sub>O<sub>2</sub>-responsive molecular fluorophore (coumarin derivative Cou-BPin) and a hydrophilic glycol chitosan and self-assembles into micellar nanoparticles in aqueous solutions. AOP **4** demonstrated high sensitivity to H<sub>2</sub>O<sub>2</sub> with a LOD of 0.1  $\mu$ M, therefore enabling imaging of endogenous H<sub>2</sub>O<sub>2</sub> in human colorectal cancer cells and facilitating the identification of circulating tumor cells (CTCs). In clinical blood samples from colorectal cancer patients, this H<sub>2</sub>O<sub>2</sub>-based CTCs counting method showed better agreement with pathological findings compared to traditional approaches.

**3.1.2. Urine.** Urine is a primary metabolite that contains various components reflecting physiological and pathological conditions, including tumor-associated biomarkers that are crucial for cancer diagnosis.<sup>75</sup> However, renal filtration and reabsorption processes significantly dilute or eliminate certain key biomolecules, presenting analytical challenges. With superior detection sensitivity and specificity, AOPs represent a promising approach to detect low-abundance urinary biomarkers.



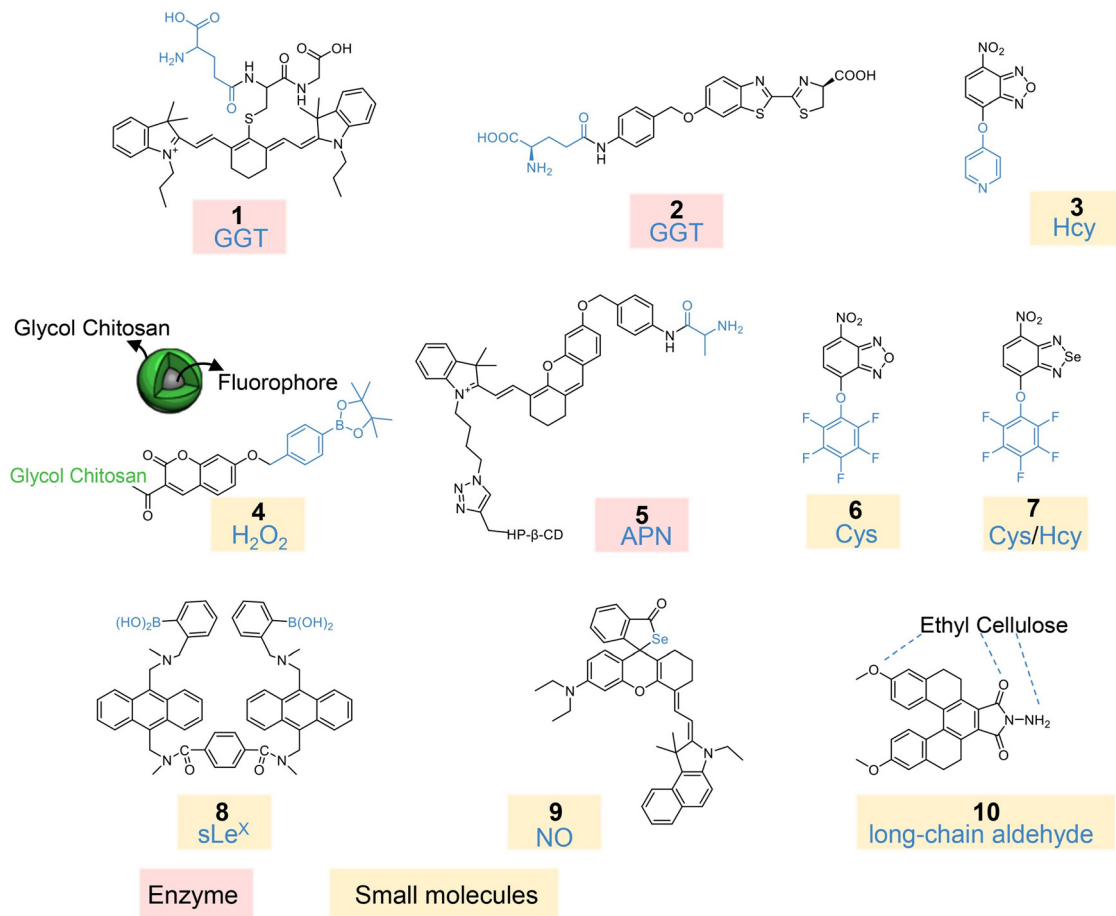


Fig. 3 Chemical structures of AOPs 1–10 for cancer diagnostics in blood (AOPs 1–4), urine (AOPs 5–8), saliva (AOP 9), and tissue fluid (AOP 10). GGT,  $\gamma$ -glutamyl transpeptidase; Hcy, homocysteine;  $\text{H}_2\text{O}_2$ , hydrogen peroxide; APN, aminopeptidase N; Cys, cysteine;  $\text{sLe}^{\text{X}}$ , sialyl Lewis X; NO, nitric oxide.

These probes are engineered to maintain minimal background signals in their initial state while generating significant signal enhancement upon biomarker recognition. The “turn-on” or ratiometric response pattern effectively reduces background signals while amplifying response signals, substantially improving the signal-to-background ratio compared to traditional “always-on” probes. As a result, AOPs enable a highly sensitive optical signal transformation, often achieving several-fold to even ten-fold signal enhancement, which ensures sensitive detection even in diluted samples. This emerging technology holds potential to advance non-invasive diagnostics, particularly in early cancer detection and disease monitoring, thereby transforming urine-based clinical assessments.

Aminopeptidase N (APN) is a membrane-bound zinc-dependent metalloprotease that is overexpressed in various cancers (bladder cancer, breast cancer, liver cancer, *etc.*).<sup>76</sup> Previously, our group reported an APN-activatable AOP 5 (Fig. 3) for sensitive bladder cancer detection.<sup>18</sup> In orthotopic bladder cancer mice model, AOP 5-based urinalysis showed a statistically significant fluorescence enhancement (2.1-fold) at 7 days post-tumor implantation, and the urine fluorescence signals continued increasing to 4.1-fold at 28 days post-tumor implantation (Fig. 4d). Histological studies further revealed

that this signal evolution correlates well with the bladder tumor progression.

Besides liable serum biomarkers, cysteine (Cys) and Hcy, are also potential urinary biomarkers for cancer detection.<sup>77</sup> Kim's group reported AOPs 6 and 7 that selectively detect urinary Cys/Hcy for cervical cancer diagnosis (Fig. 3).<sup>19,20</sup> With high sensitivity towards Cys ( $\text{LOD} = 1 \text{ ng mL}^{-1}$ ), AOP 6-based urinalysis requires a small amount of urine sample (200  $\mu\text{L}$ ) and short diagnosis time (40 min). The capability of AOP 6-based urinalysis was then tested in 1756 urine samples from well-characterized patients bearing urological disorders (urinary stone, kidney cancer, prostate cancer, and bladder cancer), non-urological disorders (cervical cancer, diabetes, pituitary adenoma, adrenal adenoma, lung cancer, ovarian cancer, pancreatic biliary tract cancer, and pancreatic cancer), and healthy controls (Fig. 4e). AOP 6 showed a remarkable performance in cervical cancer diagnosis, achieving a true positive rate of 74% and a true negative rate of 88.3% (Fig. 4f). Such a non-invasive, simple, and rapid urine-based diagnostic approach offers a promising alternative to traditional cervical cancer screening methods (pap smear and staining), potentially improving early detection rates and patients' comfort.

Sialyl Lewis X ( $\text{sLe}^{\text{X}}$ ) is a terminal O-glycan structure highly expressed on cancer cells and has been identified as a prostate



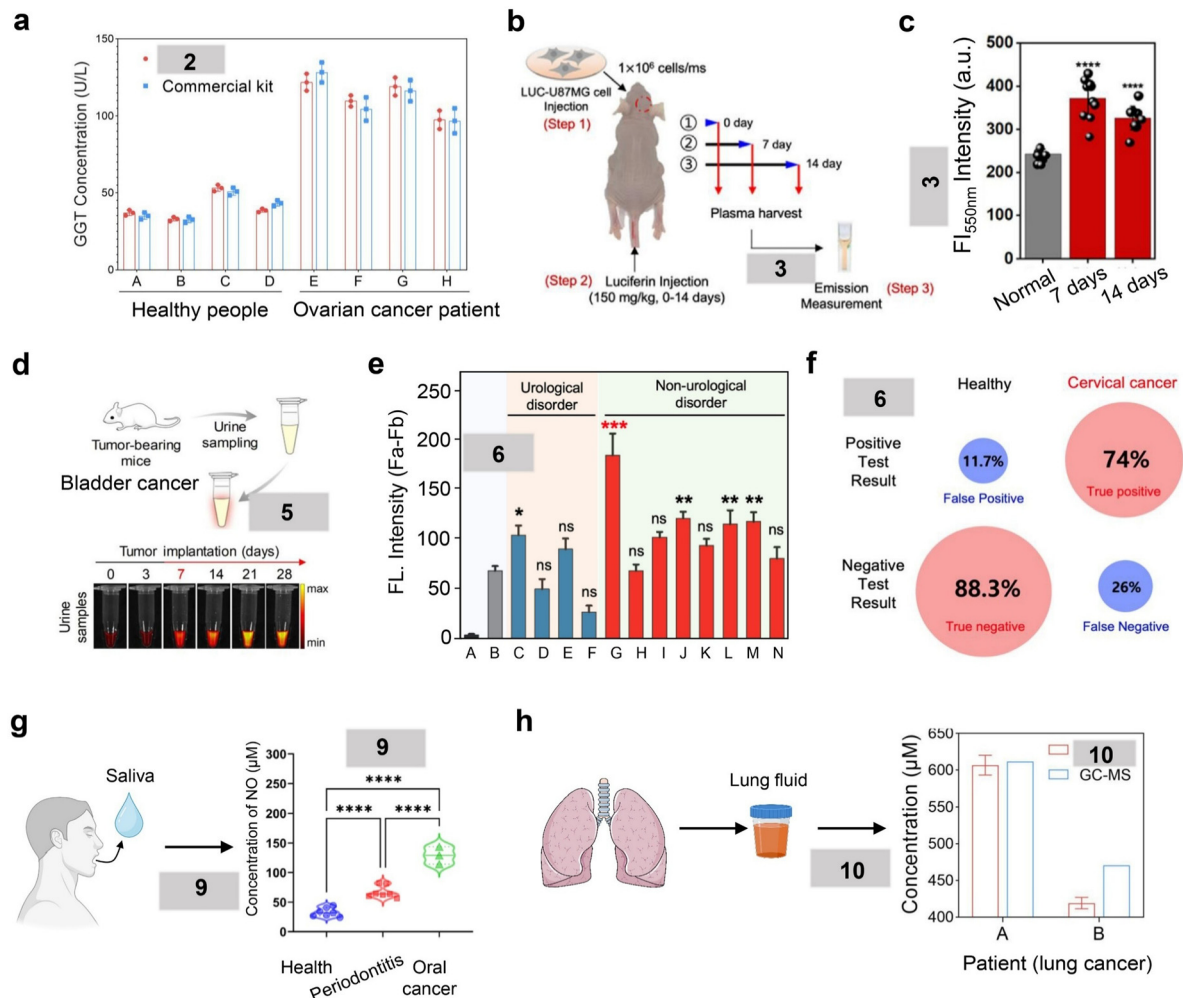


**Fig. 4** Cancer diagnostics using AOPs. Blood diagnostics: (a) comparison of serological assays using AOP **2** versus a commercial kit. Samples A–D are from healthy individuals and samples E–H are from ovarian cancer patients. (b) Experimental design showing the U87 cell xenograft mouse model and blood plasma collection timeline. (c) Fluorescence intensities of diluted plasma samples from normal and GBM mice after 10 min incubation with AOP **3**. Urine diagnostics: (d) experimental workflow for urine collection from the bladder cancer mouse model and fluorescence imaging using AOP **5**, showing progression at 0, 3, 7, 14, 21, and 28 days post-tumor implantation. (e) Fluorescence intensity of 1756 clinical urine samples after 40 min treatment with AOP **6**. Sample group: A: AOP **6** in PBS buffer, B: healthy donors ( $n = 308$ ), C: urinary stone ( $n = 162$ ), D: kidney cancer ( $n = 162$ ), E: prostate cancer ( $n = 162$ ), F: bladder cancer ( $n = 162$ ), G: cervical cancer ( $n = 100$ ), H: diabetes ( $n = 100$ ), I: pituitary adenoma ( $n = 100$ ), J: adrenal adenoma ( $n = 100$ ), K: lung cancer ( $n = 100$ ), L: ovarian cancer ( $n = 100$ ), M: pancreatic biliary tract cancer ( $n = 100$ ), and N: pancreatic cancer ( $n = 100$ ). (f) Statistical analysis of AOP **6** urinary test results showing true/false positive and negative rates for healthy donors versus cervical cancer patients. Saliva diagnostics: (g) AOP **9** detection results from saliva samples of healthy donors ( $n = 7$ ), periodontitis patients ( $n = 7$ ), and oral cancer patients ( $n = 3$ ). Tissue fluid diagnostics: (h) the workflow and quantitative comparison of nonanal in lung fluids from lung cancer patients after treatment with AOP **10** versus GC-MS analysis. Panel (a) is reproduced from ref. 15 with permission from Elsevier B.V., copyright 2017. Panels (b) and (c) are reproduced from ref. 16 with permission from Elsevier B.V., copyright 2022. Panel (d) is reproduced from ref. 18 with permission from Wiley-VCH Verlag GmbH & Co. KGaA, Weinheim, copyright 2019. Panels (e) and (f) are reproduced from ref. 19 with permission from Elsevier B.V., copyright 2022. Panel (g) is reproduced from ref. 22 with permission from Elsevier B.V., copyright 2023. Panel (h) is reproduced from ref. 23 with permission from American Chemical Society, copyright 2022.

cancer-related biomarker.<sup>78</sup> Wang and coworkers presented AOP **8**-based urinalysis for rapid prostate cancer detection.<sup>21</sup> AOP **8** selectively binds to sLe<sup>x</sup>, causing a significant fluorescence enhancement due to changes in electron transitions. With high detection sensitivity ( $\text{LOD} = 4.58 \times 10^{-10} \text{ mol L}^{-1}$ ), AOP **8**-based urinalysis successfully distinguished upregulated sLe<sup>x</sup> levels in clinical urine samples from prostate cancer patients compared to healthy controls within 15 minutes, demonstrating its potential for pancreatic cancer early screening.

**3.1.3. Saliva.** Saliva is a complex biofluid secreted by the salivary glands and comprises lots of biomolecules that reflect the systemic health. Salivary diagnostics offers several advantages, including non-invasiveness, the ease of collection, and the capacity for multiple sampling without causing patient discomfort or pain. Therefore, the saliva test has become an increasingly attractive option for diagnostic and prognostic applications. Salivary biomarkers have demonstrated significant potential as reliable diagnostic tools for a variety of pathological conditions, especially in diagnosing and monitoring diseases of



the head and oral regions. Owing to the anatomical proximity of these areas to the oral cavity, they could directly release specific biomarkers into the saliva.<sup>79</sup> This localized biomarker release mechanism could potentially enhance the sensitivity and specificity of salivary diagnostics.

Nitric oxide (NO) is a multifunctional gaseous messenger molecule involved in many important biological processes; yet, recent studies revealed that an abnormally high concentration of NO in saliva is associated with periodontitis and oral carcinoma.<sup>80</sup> Jiao *et al.* reported a novel near-infrared fluorescent probe, AOP 9 (Fig. 3), to detect the saliva NO content in clinical samples.<sup>22</sup> AOP 9 is designed based on a Se–NO bond recognition mechanism and therefore exhibits high selectivity and sensitivity towards NO with a LOD value of 28 nM. The probe demonstrates a rapid response (within 5 minutes) and near-infrared emission (780 nm), making it suitable for biological applications. The capability of AOP 9 to detect oral cancer was then evaluated with clinical experiments involving 20 saliva samples from healthy individuals and patients with periodontitis and oral cancer. In samples from oral cancer patients, the AOP 9-based saliva test showed statistically significant 4.9-, 1.9-fold fluorescence enhancements, as compared to healthy and periodontitis groups, respectively (Fig. 4g). Therefore, AOP 9 serves as a valuable tool for monitoring and evaluating the progression of oral diseases.

**3.1.4. Tissue fluid.** Tissue fluid, also known as interstitial fluid, refers to the extracellular fluid that surrounds cells within tissues, facilitating the exchange of nutrients, waste products, and signaling molecules between blood and cells.<sup>81</sup> Tissue fluid exhibits high diagnostic value as it directly reflects tissue environments; yet, it is not easily accessible for direct sampling. Recently, with advances in clinical techniques (microdialysis, pressure measurements, artificial lavage, analysis of wound exudates, *etc.*), tissue fluid-based *in vitro* diagnosis provides insights into local physiological and pathological processes, complementing traditional blood and urine tests in both clinical and preclinical applications.<sup>82</sup>

For example, long-chain aldehydes (specifically, hexanal, heptanal, octanal, and nonanal) have been identified as significant biomarkers for lung cancer diagnosis, and their concentrations in biological matrices (lung fluid, blood, tumor tissue, and exhaled breath) exhibit up to 80% elevation in lung cancer patients compared to healthy individuals.<sup>83</sup> To achieve the specific detection of long-chain aldehydes, Jongkhumkrong *et al.* presented a novel fluorescent nanosensor, AOP 10 (Fig. 3) based on helicene dye encapsulated in ethyl cellulose.<sup>23</sup> The helicene dye contains a hydrazide group and could react with the aldehyde group *via* imine formation; the chemical conjugation along with hydrophobic interactions with alkyl long-chain aldehydes subsequently induce nanosensor self-assembly and fluorescence turn-ON. AOP 10 showed high selectivity and sensitivity with a short measurement time (15 minutes) and a LOD value of 10  $\mu$ M towards nonanal. The capability of AOP 10 to quantify long-chain aldehyde content in lung fluid samples was then tested with clinical specimens from lung cancer patients, and the fluorescence enhancement from AOP 10 showed a

positive correlation with standard gas chromatography–mass spectrometry (GC-MS) (Fig. 4h). Therefore, with the advantages of high specificity, rapid response time, and simplicity of use, AOP 10 could become a promising tool for both research and clinical diagnostics in lung cancer management.

### 3.2. Nephro-urological disorders

Nephro-urological disorders encompass a wide range of conditions affecting the kidneys, ureters, bladder, and urethra and represent a significant global health concern.<sup>84</sup> Current clinical approaches employ a combination of laboratory tests, imaging techniques, and invasive biopsy. In comparison to other clinical methods, *in vitro* diagnostics provides a non-invasive and rapid test approach; yet, it is limited by issues of poor sensitivity and specificity, particularly in early-stage disease detection.<sup>85</sup> To resolve these limitations, the AOP-based urine test with enhanced specificity and real-time result readout capabilities could potentially improve disease early detection and personalized treatment strategies in nephro-urological disorders.

**3.2.1. Urine.** Urine possesses unique physiological properties that reflect real-time alterations in urological homeostasis and pathogenic changes in the nephron-urological system.<sup>86</sup> Therefore, urine serves as the representative biofluid for urological disease diagnostics. In particular, urine contains numerous biomarkers (small molecules, enzymes, proteins, *etc.*) that are indicative of renal functions, metabolic processes, and pathological conditions, providing a rich source of diagnostic information for urological diseases.<sup>87</sup> Therefore, urinary biomarker-responsive AOPs have been developed and applied for early diagnosis and management of urinary system disorders, for example, real-time monitoring of kidney functions, early detection of kidney diseases, and rapid drug screening.

Monitoring up-regulated urinary enzymes provides a non-invasive approach to detect renal dysfunctions at an early stage before kidney structural damages as reflected by elevations in serum creatinine.<sup>88</sup> A series of AOPs have been developed to detect urinary enzymes that are associated with key pathophysiological processes, such as lysosomal damages (*N*-acetyl- $\beta$ -D-glucosaminidase (NAG))<sup>89</sup> and proximal tubule brush border membrane damages (GGT, alanine aminopeptidase (AAP), and dipeptidyl peptidase-IV (DPP-IV)).<sup>90</sup> Previously, our group designed AOPs 11–13 for sensitive detection of drug-induced kidney injury (DIKI) at an early disease stage.<sup>24,25</sup> These AOPs were constructed by caging the optically tunable atoms on fluorophores (coumarin, resorufin, and hemi-cyanine) with biomarker-responsive groups (GGT:  $\gamma$ -glutamate; AAP: alanine; NAG: *N*-acetyl- $\beta$ -D-glucosaminide). The capabilities of AOPs 11–13 to detect kidney dysfunctions were then tested in pre-clinical DIKI mice models in both acute and chronic manners. In cisplatin-induced acute kidney injury mice model, NAG-activatable AOP 11 detected the onset of kidney injuries at 24 hours post-cisplatin treatment, which was at least 24 hours earlier than other preclinical blood and urine biomarkers (cystatin C, neutrophil gelatinase-associated lipocalin, osteopontin,  $\beta$ 2-microglobulin, and trefoil factor-3), and 48 hours earlier than clinical serum creatinine and the BUN test.



For multiplex urinalysis, AOPs **11–13** were designed to emit distinct fluorescence signals with a minimal overlap (Fig. 6a–c). In doxorubicin-induced chronic kidney disease models, these AOPs detected kidney dysfunction 5 days earlier than traditional clinical biomarkers like serum creatinine and blood urea nitrogen (Fig. 6d and e). Besides, as shown in Fig. 6f, receiver operating characteristic (ROC) analysis revealed that AOPs (**11–13**)-based multiplex urinalysis demonstrated the highest diagnostic accuracy (AUC = 0.94) among traditional clinical diagnostic approaches (AUC  $\approx$  0.75).

In addition, enzyme-activatable AOPs have been applied for nephron-urological disease diagnostics using clinical specimens. For example, Isomoto *et al.* developed AOPs **14 and 15** that are specific towards DPP-IV and GGT and demonstrated their applications in diabetic kidney disease diagnosis.<sup>26</sup> Both DPP-IV and GGT are localized to proximal tubular cells, and are released into urine when tubules are injured; yet both tubular and circulating DPP-IV are up-regulated in patients with diabetes mellitus. In a clinical study involving 102 patient urine samples, AOPs (**14 and 15**)-based urinalysis successfully differentiated diabetic kidney diseases from nephrosclerosis or glomerulonephritis. Therefore, the non-invasive nature, early detection capability, and improved diagnostic accuracy make these urinalysis approaches promising for both preclinical drug screening and clinical diagnosis of nephron-related diseases.

Detection of abnormal levels of urinary protein (especially albumin (ALB)) holds great clinical importance, as it reflects

various disease states such as kidney injuries, diabetic nephropathy, cardiovascular risk, and pregnancy complications.<sup>91</sup> However, clinical methods to detect urine proteins, including dipstick tests, immunoturbidimetry, and immunofluorescence imaging suffer from shortcomings such as low sensitivity, insufficient specificity, and complicated operation procedures. To address these challenges, researchers have developed a series of AOPs **16–20** to achieve sensitive detection of urinary proteins (Fig. 5).<sup>13,27–30</sup> For example, Zhou's group reported AOP **17** to quantitatively detect urinary ALB in samples from chronic kidney injury rat models and patient samples.<sup>28</sup> AOP **17** specifically binds to the hydrophobic cavity of ALB which inhibits the TICT effect, and the fluorescence intensity responds linearly towards ALB concentrations (0 to 1.0 g L<sup>-1</sup>) with a LOD of 0.36 mg L<sup>-1</sup> (5.4 nM). AOP **17** was then applied to quantify the ALB amount in patient samples, and showed consistent results with the Coomassie Brilliant Blue staining method (Fig. 6g).

Zhu *et al.* reported AOP **20** for POCT of urinary microalbumin (mALB) in clinical patient samples.<sup>13</sup> AOP **20** exhibited conformational changes upon binding to mALB, transitioning from a twisted structure to a more planar one, which subsequently mitigated the TICT effect with fluorescence activation. *In vitro* experiments revealed that AOP **20** achieves mALB detection with a wide linear range (0–8000  $\mu$ g mL<sup>-1</sup>) and a low LOD (3.1501  $\mu$ g mL<sup>-1</sup>). Subsequently, AOP **20** was applied for POCT (Fig. 6h). As shown in Fig. 6i, AOP **20**-based POCT ( $\Delta F$ )

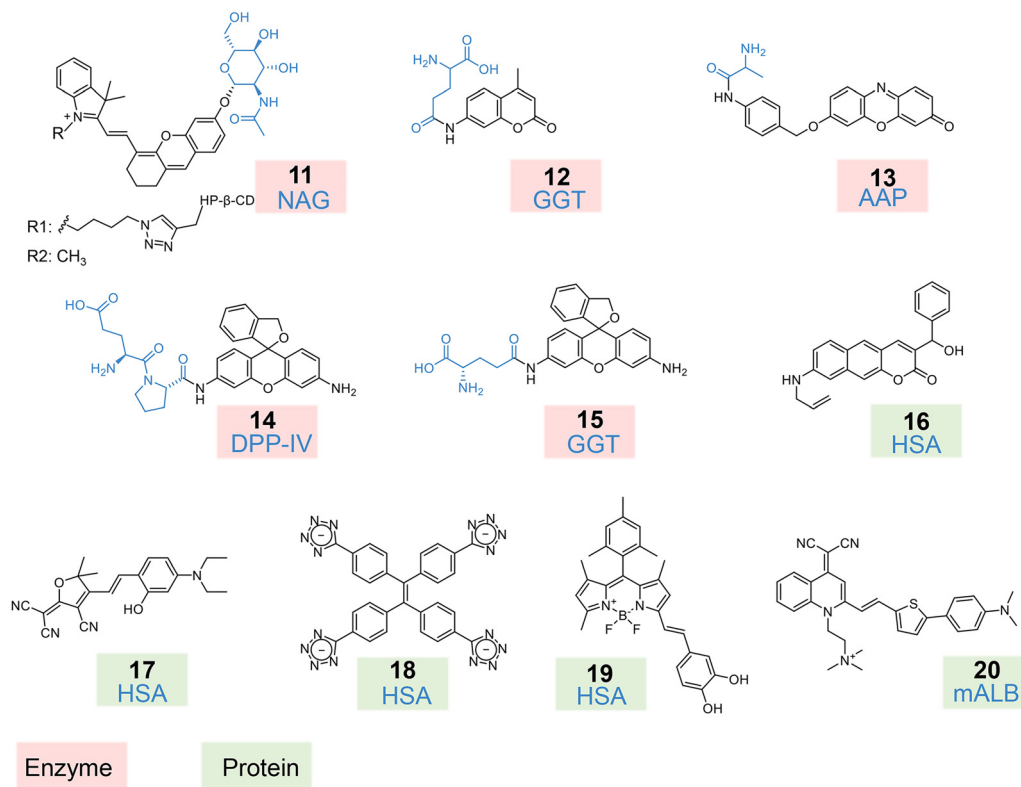
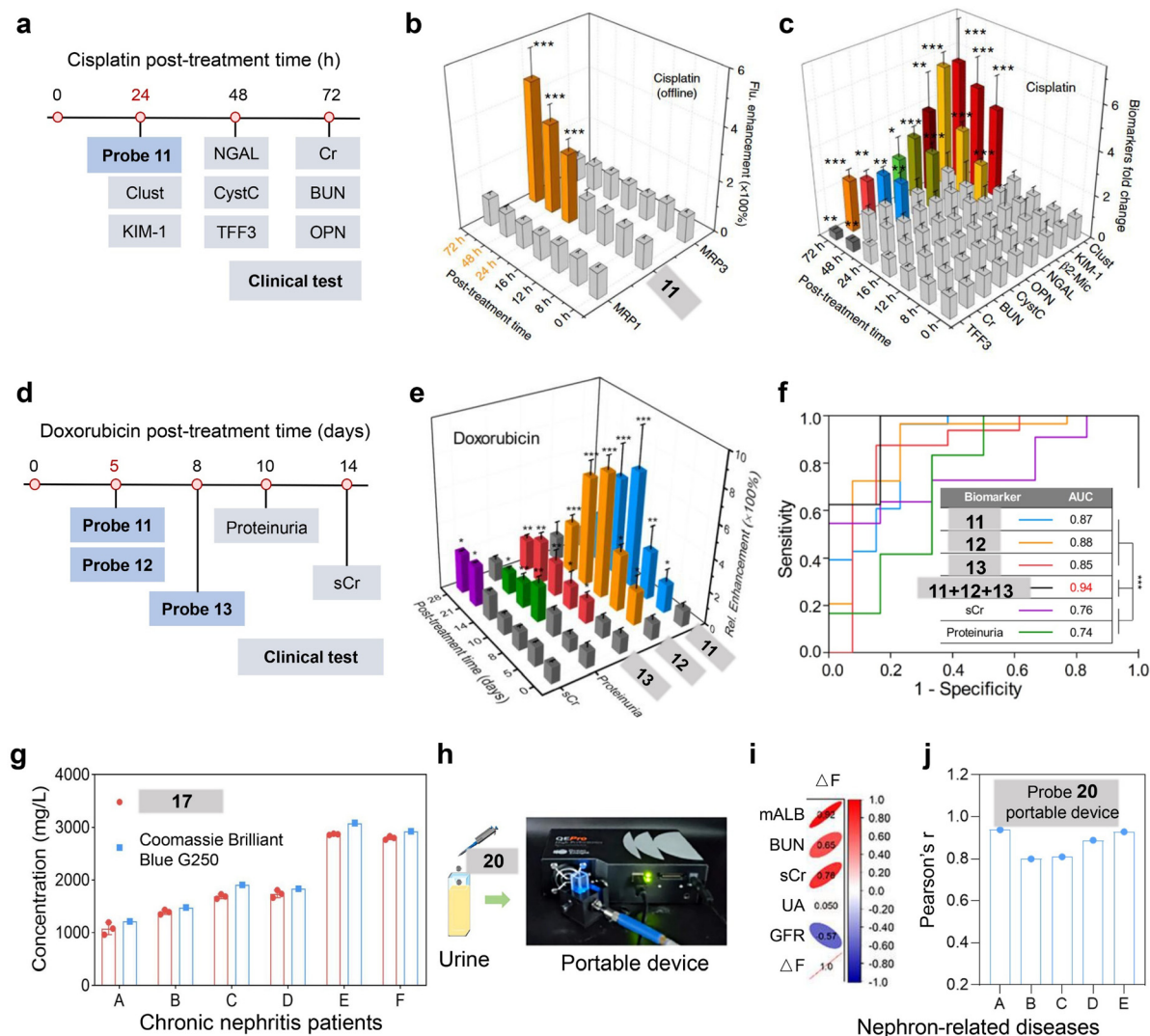


Fig. 5 Chemical structures of AOPs **11–20** for nephron-urological disorder diagnostics in urine. NAG, *N*-acetyl- $\beta$ -D-glucosaminidase; GGT,  $\gamma$ -glutamyl transpeptidase; DPP-IV, dipeptidyl peptidase-IV; HSA, human serum albumin; mALB, microalbumin.





**Fig. 6** Nephro-urological disorders diagnostics using AOPs. (a) Comparative timeline of AOP **11**-based urinalysis *versus* conventional clinical biomarkers for the detection of drug-induced AKI. (b) Fluorescence enhancement of AOP **11** in urine samples from drug-treated mice at various post-treatment time points (mean  $\pm$  s.d.,  $n = 9$ ). (c) Fold change in urinary and serum biomarker levels following drug treatment. (d) Comparative timeline showing AOPs **11**–**13**-based urinalysis *versus* clinical biomarker detection for the detection of drug-induced AKI. (e) Fluorescence enhancement of AOPs **11**–**13** and clinical biomarker detection after incubation with drug treatment ( $n = 5$ , mean  $\pm$  s.d.). (f) ROC curve analysis comparing diagnostic performance between individual AOPs (**11**, **12**, **13**), their combination (**11** + **12** + **13**), and conventional markers (sCr and proteinuria) in distinguishing nephrotoxicant-treated animals with renal injuries from untreated controls. (g) HSA level quantification in chronic nephritis patient urine samples using AOP **17** *versus* the standard Coomassie Brilliant Blue G250 method ( $n = 3$ ). (h) Schematic workflow of the AOP **20**-based portable device for urinary analysis. (i) Heat map showing correlations between  $\Delta F$  (fluorescence intensity of urine with AOP **20** at 750 nm – fluorescence intensity of urine at 750 nm) and clinical markers, and  $\Delta F$  shows high correlations with mALB (Pearson's  $r = 0.92$ ). mALB, microalbuminuria; BUN, blood urea nitrogen; sCr, serum creatinine; UA, blood uric acid; GFR, glomerular filtration rate. (j) Pearson correlation analysis of the AOP **20**-based portable device across various nephron-related diseases (A: chronic nephritis, B: type 2 diabetes, C: high blood pressure, D: nephropathy, E: chronic renal failure). Panels (a)–(c) are reproduced from ref. 24 with permission from Springer Nature Limited, copyright 2019. Panels (d)–(f) are reproduced from ref. 25 with permission from American Chemical Society, copyright 2020. Panel (g) is reproduced from ref. 28 with permission from Elsevier B.V., copyright 2023. Panels (h)–(j) are reproduced from ref. 13 with permission from SCUT, AIEI and John Wiley & Sons Australia, Ltd, copyright 2024.

showed the strongest positive correlation with mALB levels (Pearson's  $r = 0.92$ ) than other kidney functional markers (BUN, sCr, UA, and GFR). Furthermore, AOP **20**-based POCT showed positive correlation with the clinical ELISA method (Pearson's  $r = 0.8$ – $0.9$ ) across different nephron-related diseases (chronic nephritis, type 2 diabetes, high blood pressure, nephropathy, and chronic renal failure), validating its

reliability for practical applications (Fig. 6j). This comprehensive evaluation confirms the potential of AOP **20** as a reliable POCT tool for kidney-related diseases.

### 3.3. Infectious diseases

Infectious diseases are primarily caused by pathogenic microorganisms such as bacteria, viruses, fungi, and parasites and



have posed significant global health challenges.<sup>92</sup> Therefore, rapid and accurate diagnostic approaches are essential to achieve effective treatment and prevention of spread. Traditional clinical diagnostic approaches such as culture-based techniques and PCR often face limitations including time-consuming processes, limited sensitivity, and high costs.<sup>93</sup> In contrast, AOPs that detect antimicrobial resistance markers with high sensitivity and specificity have been readily developed, and AOP-based body fluid diagnostics offers several advantages for infectious disease diagnosis, such as rapid results, direct visual readout, quantitative assessment, and minimal sample requirement. Thus, AOPs have potential to become valuable tools for improving infectious disease diagnosis in clinical settings.

**3.3.1. Sputum.** Sputum is a complex biofluid produced in the lung and respiratory tract, and contains a rich array of biomolecules that reflect the health status of the respiratory system.<sup>94</sup> Sputum, as biological specimen, offers unique advantages for diagnostic purposes, including its non-invasive nature, ease of collection, and the ability to obtain multiple samples without causing significant patient discomfort.<sup>95</sup> In addition, as a result of the direct contact between sputum and the affected respiratory tissues, sputum biomarkers could serve as reliable diagnostic tools for a variety of respiratory conditions, such as pneumonia, tuberculosis, and cystic fibrosis.<sup>94</sup> Therefore, sputum-based disease diagnostics has become an indispensable detective tool in respiratory medicine.

Tuberculosis, an infectious lung disease caused by *Mycobacterium tuberculosis* (Mtb) infection, remains one of the most deadly diseases with high morbidity and mortality.<sup>96</sup> Therefore, the precise detection of Mtb is crucial for early diagnosis and treatment efficacy monitoring of pulmonary infections. Liu *et al.* reported AOP 21 that specifically activates fluorescence in response to Rv3368c, and Rv3368c is a specific nitroreductase conversely expressed in live Mtb.<sup>31</sup> AOP 21 is designed by incorporating a cyanine fluorophore with a nitrobenzyl group which acts as a PET quencher. In *in vitro* experiments, AOP 21 showed high detection specificity and sensitivity towards Rv3368v-positive Mtb in sputum, with LODs of  $3.5 \times 10^2$  and  $4.3 \times 10^2$  CFU, respectively, for *M. smegmatis*, Mtb H37Rv. The AOP 21-based sputum test was then applied for TB diagnosis using clinical samples, and showed both high sensitivity (85.9%) and specificity (99.0%) in distinguishing TB patients from healthy donors (Fig. 8a). As compared to the clinical BACTEC MGIT 960 culture methods or auramine O (AO) bacterial staining, AOP 21 showed similar diagnostic accuracy, yet significantly reduced detection time (15 min to 2 hours), prolonged signal retention time (24 hours) and superior photostability (Fig. 8b).

Besides Rv3368c,  $\beta$ -lactamase (BlaC, class A  $\beta$ -lactamase) is an enzyme naturally expressed and secreted by Mtb. To achieve sensitive detection of BlaC, Rao's group reported AOP 22 and demonstrated their applications in the diagnosis of tuberculosis in clinical sputum specimens.<sup>12</sup> AOP 22 was constructed based on chemically modified cephalosporins; and upon BlaC hydrolyzation, they release free umbelliferone with up to

200 fold fluorescence enhancement. This allowed for rapid detection of Mtb var. *bovis* strain BCG (<10 CFU) in the unprocessed human sputum within 10 minutes. The potential of AOP 22 for POCT technique was then demonstrated with a cell phone-implemented portable device, and similar detection sensitivity was observed (Fig. 8c).

An alternative approach for detecting Mtb involves targeting specific enzymes and structural components of the bacterium. On the basis of AOP 22, Rao's group further reported a dual-targeting AOP 23 that could both fluoresce upon BlaC activation and retain covalent binding towards DprE1 (involved in cell wall synthesis) to label single bacilli and signal retention.<sup>32</sup> With dual-targeting capability, AOP 23 not only differentiated live from dead Mtb var. *bovis* BCG strains, but also showed specificity for Mtb over other bacterial species. AOP 23 was then applied in patients' sputum imaging, and recognized Mtb strains in a GeneXpert (commercial DNA detection method) positive but the auramine O (stain with mycolic acids) negative sample (Fig. 8d). The authors further incorporated AOP 23 into a low-cost, self-driven microfluidic chip, and demonstrated its potential for POCT with rapid, automated quantification of live BCG in patient sputum. Similarly, Bertozzi's group reported AOP 24, which could be catalyzed by antigen 85 (Ag85, is a complex of enzymes crucial for *Mycobacterium tuberculosis* and plays a vital role in cell wall synthesis) into the mycomembrane as trehalose mycolates.<sup>33</sup> Upon incorporation, the fluorophore transitions from an aqueous to a hydrophobic environment within the mycomembrane, triggering a >700-fold increase in fluorescence. This process allows specific labeling of live Mtb without washing steps, with a LOD value of approximately  $10\,000\text{ CFU mL}^{-1}$  in sputum. AOP 24 was then applied to detect Mtb in clinical patient samples, and showed comparable diagnostic accuracy to clinical auramine O staining yet much simpler operational protocol (Fig. 8e).

**3.3.2. Synovial fluid.** Synovial fluid, a viscous substance found within the cavities of synovial joints, is produced by the synovial membrane and contains a complex mixture of components (hyaluronic acid, lubricin, proteinases, and collagenases) that collectively maintain joint health and functions. Although the collection of synovial fluid involves invasive procedures, its unique composition offers a significant diagnostic value and it directly reflects the physiological and pathological conditions of the joint environment.

Septic arthritis is an infectious orthopaedic disease mainly caused by *Staphylococcus aureus* (*S. aureus*),<sup>97</sup> and AOPs responsive towards *S. aureus*-specific enzymes have been developed for disease detection. Micrococcal nuclease is an enzyme specifically secreted by *S. aureus* and widely used in molecular biology for chromatin studies, nucleic acid cleanup, therefore serving as a diagnostic marker for *S. aureus*. Van Dijk *et al.* reported AOP 25 (Fig. 7) which consists of a fluorophore (ATTO488) and quencher (ZEN-IAbRA) pair linked by a nuclease-cleavable oligonucleotide.<sup>34</sup> After incubation with clinical synovial fluid (biofilm) samples, AOP 25 distinguishes *S. aureus* from other bacteria within 2 hours (15 min), which provides a much more rapid approach as compared to traditional culture methods



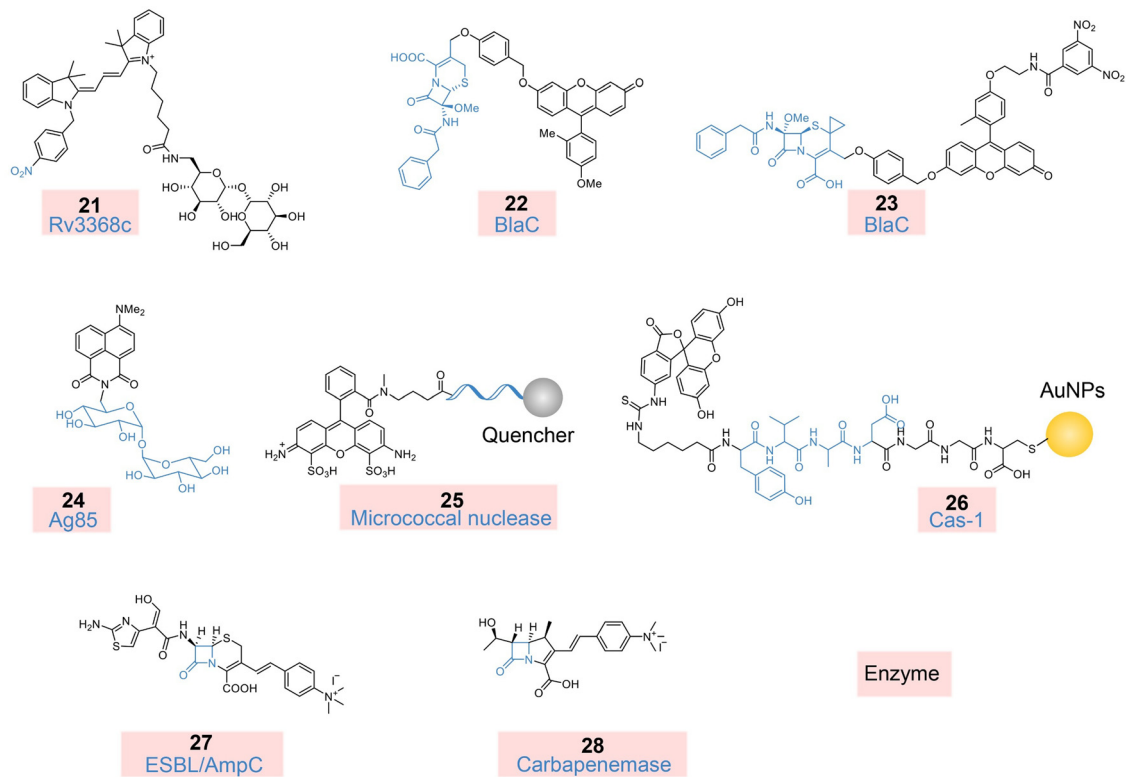


Fig. 7 Chemical structures of AOPs **21–28** for infectious disease diagnostics in sputum (AOPs **21–24**), synovial fluid (AOPs **25, 26**) and urine (AOPs **27, 28**). Rv3368c, nitroreductase Rv3368c; BlaC,  $\beta$ -lactamase; Ag85, antigen 85; Cas-1, caspase-1; ESBL/AmpC, extended-spectrum/AmpC  $\beta$ -lactamases.

(2–5 days). Thus, AOP **25** showed potential for real-time, intra-operative visualization of *S. aureus* infection.

In addition, the bacterial immune escape in host cells (especially in macrophages) frequently causes ineffective antibiotic treatment effects and disease recurrence of septic arthritis.<sup>98</sup> To achieve rapid and sensitive detection of intracellular bacteria, Song and coworkers reported an activatable fluorescent AOP **26** that triggers fluorescence signals in response to caspase-1 (Cas-1), which is a cysteine protease expressed in bacterial-infected macrophages.<sup>35</sup> AOP **26** was constructed by conjugating FITC and gold nanoparticles (AuNPs), respectively, as energy donors and acceptors, *via* a Cas-1-cleavable peptide sequence. AOP **26** exhibited high detection specificity and sensitivity with a LOD of 5 *S. aureus* per host cell without the need for washing extracellular bacteria. AOP **26** was then applied to detect intracellular bacteria in patients' synovial fluid samples, and its activated fluorescence signals showed a positive correlation with bacterial colony growth, demonstrating the diagnostic potential of AOP **26** (Fig. 8f).

**3.3.3. Urine.** Urinary tract infections (UTIs) are the most common nosocomial infection affecting millions globally. Urinary tests serve as essential tools in diagnosing, monitoring, and managing UTIs, providing critical information about bacterial infection, inflammation response, and therapeutic efficacy. Traditional diagnostic methods require 2–5 days for bacterial culture and antimicrobial susceptibility testing, making rapid detection critical for improving patient outcomes.<sup>99–101</sup> BlaC, including extended-spectrum/AmpC  $\beta$ -lactamases (ESBL/AmpC)

and carbapenemases, is a major factor causing antibiotic resistance in bacteria, particularly in UTI treatment. Liu's group reported AOPs **27** and **28** for simultaneous ESBL/AmpC and carbapenemase detection and demonstrated their applications in the diagnosis of UTIs with clinical samples.<sup>36</sup> These probes were designed based on the ICT effect, where BlaC catalyzes the hydrolysis of the carbon-nitrogen bond in the  $\beta$ -lactam structure, leading to decreased structural rigidity and electron movements, with corresponding color changes from light-green to red visible to naked eye. AOPs **27** and **28** were applied in a paper sensor and achieved a LOD value of  $5 \times 10^4$  CFU mL<sup>-1</sup> for  $\beta$ -lactamase-producing bacteria. In clinical validation with 30 UTI patient samples, the paper sensor successfully identified 10 cases as ESBL/AmpC-positive and 8 cases as carbapenemase-positive, showing 100% clinical sensitivity and specificity compared to clinical laboratory results. The entire detection process could be completed within 5 minutes, providing a rapid solution for UTI diagnosis and rational antibiotic prescription, particularly valuable in resource-limited settings.

### 3.4. Digestive diseases

Digestive diseases refer to disorders occurred in the gastrointestinal tract, liver, pancreas, and associated organs, and represent a significant global health burden.<sup>102</sup> Digestive disorders can manifest in diverse forms, ranging from chronic inflammation to liver cirrhosis and even cancer. Therefore, the complex nature of these diseases necessitates accurate and timely diagnosis for effective management and prevention of complications.



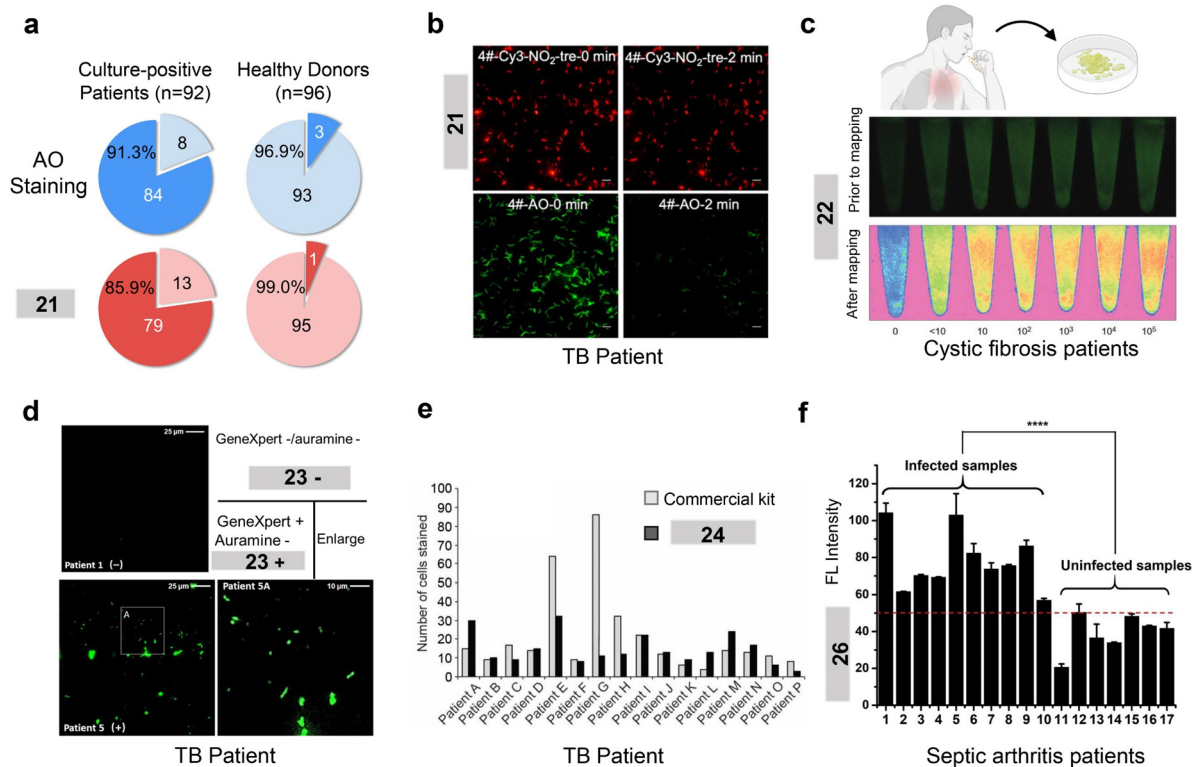


**Fig. 8** Infectious disease diagnostics using AOPs. (a) Comparative detection sensitivity of Rv3368c in sputum samples using AOP **21** versus conventional AO staining. Pie charts show detection rates in culture-positive TB patients ( $n = 92$ ) and healthy donors ( $n = 96$ ). AO, auramine O. (b) Time-lapse fluorescence microscopy images of TB positive sputum samples treated with AOP **21** or AO. (c) Fluorescence imaging and (pre/after)-mapping results using a smart phone of BCG-spiked sputum samples from cystic fibrosis patients and incubated with AOP **22**. (d) Comparative *Mtb* detection in sputum samples using GeneXpert, AO smear staining and AOP **23** staining, respectively. Patient 1 (negative in all tests); patient 5 (GeneXpert+/auramine-). (e) Quantitative comparison of *Mtb* cell detection efficiency between AOP **24** and commercial AO staining across 16 sputum samples. (f) Fluorescence intensity of synovial fluid samples from septic arthritis patients after AOP **26** treatment, with a red dashed line indicating a diagnostic threshold, \*\*\*\* $p < 0.0001$ . Panels (a) and (b) are reproduced from ref. 31 with permission from American Chemical Society, copyright 2024. Panel (c) is reproduced from ref. 12 with permission from Springer Nature Limited, copyright 2012. Panel (d) is reproduced from ref. 32 with permission from American Association for the Advancement of Science, copyright 2018. Panel (e) is reproduced from ref. 33 with permission from American Association for the Advancement of Science, copyright 2018. Panel (f) is reproduced from ref. 35 with permission from Elsevier B.V., copyright 2024.

While current diagnostic methods such as endoscopy, imaging techniques, and clinical laboratory tests have been crucial in identifying these conditions, they often present challenges including invasiveness, high costs, professional operators, and limited sensitivity. In response to these limitations, AOP-based body fluid diagnostics offers promising advantages for digestive disease diagnosis, including minimal-invasion, rapid results, high sensitivity and specificity, visual readout, and simplified detection processing. The application of AOP-based body fluid diagnostics for digestive diseases enables more precise and personalized treatment strategies, and ultimately improving patient outcomes.

**3.4.1. Blood.** Hematological tests play a crucial role in diagnosing, monitoring, and prognosis for digestive diseases, offering valuable insights into inflammation, nutrition, organ function, and potential malignancies.<sup>103</sup> Zhang's and Liu's groups reported AOPs **29–30** to achieve liver cirrhosis diagnosis via the blood test (Fig. 9).<sup>37,38</sup> In terms of biomarker selection, leucine aminopeptidase (LAP) and monoamine oxidase (MAO) are selected as they are biomarkers for hepatocyte injuries and

upregulated oxidative stress in cirrhosis, respectively. AOP **29** is a “tandem-lock” probe that could be sequentially activated by LAP and MAO with a linear detection range of  $0\text{--}20 \text{ U L}^{-1}$ . In serum tests with clinical patient samples, AOP **29** successfully distinguished cirrhotic and hepatitis B patients from healthy control samples, with 3.3 and 1.8-fold fluorescence enhancements, respectively (Fig. 10a). Similarly, Liu *et al.* reported AOP **30** for the simultaneous detection of LAP and MAO based on an AND-logic gate. AOP **30** exhibits high detection sensitivity with LOD values of  $0.249$  and  $0.877 \text{ U L}^{-1}$  for MAO and LAP, respectively. In clinical serum tests, AOP **30** differentiated cirrhotic patients from healthy individuals and hepatitis B patients with a high signal-to-background ratio (Fig. 10b). Compared to conventional clinical methods, AOPs **29** and **30** offer advantages, such as higher specificity due to their dual-enzyme activation mechanism, reduced false-positive results, and the ability to differentiate liver diseases.

Acute pancreatitis is an inflammatory disease caused by premature activation of digestive enzymes within the pancreas leading to autodigestion and severe inflammation and remains



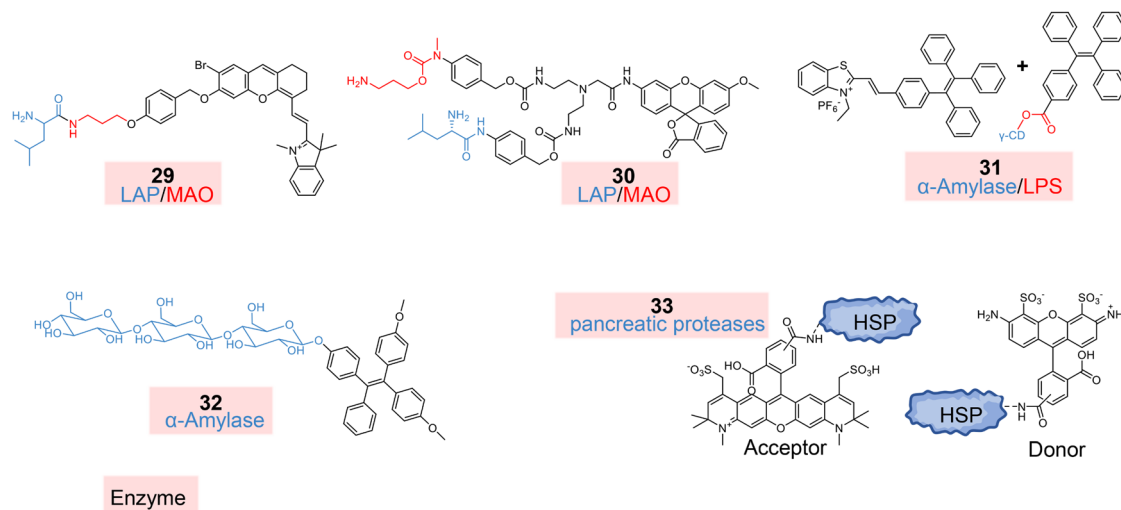


Fig. 9 Chemical structures of AOPs **29–33** for digestive system disease diagnostics in blood (AOPs **29–32**) and drainage fluid (AOP **33**). LAP, leucine aminopeptidase; MAO, monoamine oxidase; LPS, lipase; HSP, heat shock protein.

one of the most severe abdominal emergencies with high mortality, making early detection and appropriate therapeutic intervention critical for improving patient outcomes.<sup>104</sup> Lipase (LPS) and  $\alpha$ -amylase (AMY) are enzymes produced by the pancreas and elevated circulating enzyme levels in body fluids are commonly associated with pancreatic inflammation or damage. Therefore, lipase and  $\alpha$ -amylase have become key indicators for diagnosing acute pancreatitis in clinical settings; yet rapid and sensitive detection approaches are still lacking. Tang's group presented AOPs **31** and **32** (Fig. 9) for simultaneous LPS and AMY detection and demonstrated their applications in the diagnosis of acute pancreatitis with clinical samples.<sup>39,40</sup> AOP **31** was a supramolecular complex consisting of TPE- $\gamma$ -CD and TPE-H designed to operate in a homogeneous system, enabled by the  $\gamma$ -CD cavity creating a micro hydrophilic-hydrophobic interface, eliminating the need for complex two-phase systems. AOP **31** exhibited dual fluorescence responses with minimal crosstalk: blue emission (460 nm) for lipase and orange emission (610 nm) for  $\alpha$ -amylase, with excitation at 390 nm. Upon incubation with LPS/AMY, AOP **31** exhibits rapid responses and visible color changes could be observed within 25 min. The LODs were determined to be  $0.11 \text{ U L}^{-1}$  and  $0.17 \text{ U L}^{-1}$  for lipase and  $\alpha$ -amylase, respectively. Besides, AOP **31**-based clinical serum tests enable clear differentiation of acute pancreatitis patients from healthy individuals, and the results coincided with those of the commercial lipase assay kit and  $\alpha$ -amylase assay (Fig. 10c). To further improve detection sensitivity, the same group reported an AIE-based AOP **32** to detect AMY. AOP **32** showed high detection sensitivity towards  $\alpha$ -amylase with a LOD of  $0.14 \text{ U L}^{-1}$  and a response time of just 3 minutes. AOP **32** was then applied to test clinical samples (serum, urine, and saliva) for acute pancreatitis diagnosis and psychological stress analysis, and demonstrated high detection accuracy.

**3.4.2. Drainage fluid.** Drainage fluid is a biological fluid collected from surgical sites or body cavities, and is produced in response to tissue injury, inflammation, or pathological

processes. Therefore, it typically contains a complex mixture of components, including inflammatory mediators, cellular debris, proteins, enzymes, and potentially microorganisms, which collectively reflect the healing status and potential complications. While its collection typically requires invasive procedures such as surgical drain placement or needle aspiration, the unique composition of the drainage fluid offers significant diagnostic value, as it directly reflects the local tissue environment, inflammatory responses, and potential pathological processes occurring at the collection site.

Pancreatic proteases (such as trypsin, chymotrypsin, elastase) are digestive enzymes produced by the pancreas that break down proteins in the small intestine. Following gastroenterological surgeries, postoperative pancreatic fistula (POPF) represents a severe complication. Elevated levels of pancreatic proteases in post-surgical drainage fluid serve as crucial indicators for early detection and risk assessment of POPF development.<sup>105</sup> Hashizume *et al.* presented a novel nanoprobe AOP **33** (Fig. 9) with a heat shock protein (HSP) nanocage labeled with donor and acceptor fluorophores, which used FRET disruption upon cleavage by pancreatic proteases in the drainage fluid.<sup>41</sup> AOP **33** possessed a rapid response time of 10 minutes, and LOD values as low as  $0.003 \text{ U mL}^{-1}$  for elastase,  $5.00 \text{ U mL}^{-1}$  for trypsin, and  $0.02 \text{ U mL}^{-1}$  for  $\alpha$ -Chymotrypsin. AOP **33** demonstrated superior performance in differentiating POPF drainage fluid samples from normal samples. Its unique advantages include simultaneous detection of multiple pancreatic proteases, higher stability in blood plasma, lower toxicity, and the ability to provide visual detection visible to the naked eye under UV light (Fig. 10d). Compared to conventional methods like amylase measurements, this approach offers faster, more specific results and the potential for intraoperative visualization of pancreatic juice leakage.

### 3.5. Other diseases

**3.5.1. Blood.** Coronary heart disease (CHD) is a progressive atherosclerotic pathology characterized by the accumulation of



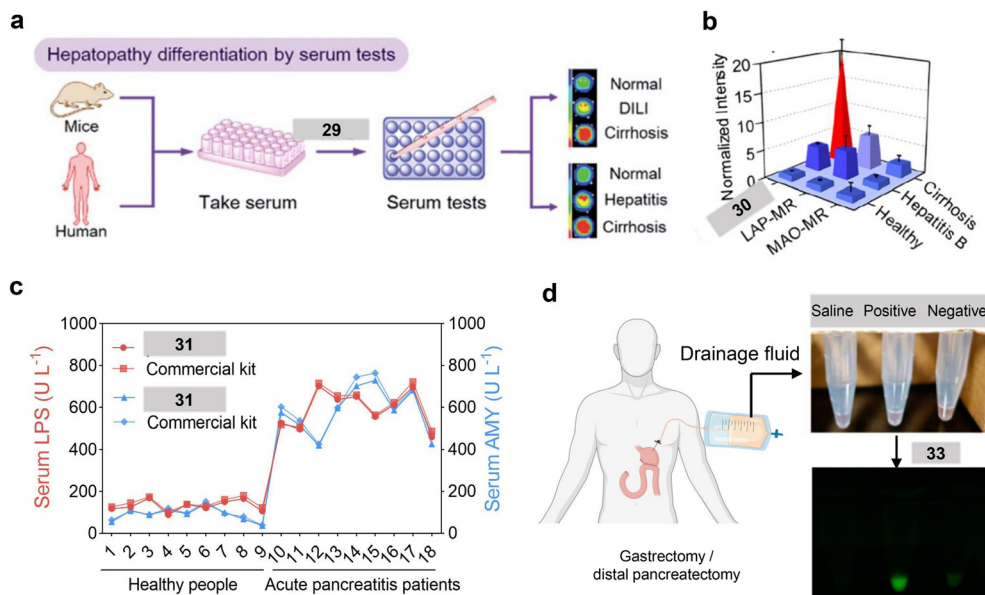


**Fig. 10** Digestive disease diagnostics using AOPs. (a) Schematic workflow of hepatopathy differentiation using AOP **29**-based serum testing in both mouse and human samples. (b) Comparative analysis of fluorescence intensity in human serum samples from healthy individuals, hepatitis, and cirrhosis patients using AOP **30** and compared probes. (c) Comparison of endogenous LPS and AMY activity in serum samples from healthy individuals and acute pancreatitis patients, measured by AOP **31** versus the commercial kit. LPS, lipase; AMY,  $\alpha$ -amylase. (d) Photograph and fluorescence images of drainage fluid from gastrectomy/distal pancreatectomy patients using AOP **33**. Panel (a) is reproduced from ref. 37 with permission from The Royal Society of Chemistry, copyright 2019. Panel (b) is reproduced from ref. 38 with permission from The Royal Society of Chemistry, copyright 2019. Panel (c) is reproduced from ref. 39 with permission from American Chemical Society, copyright 2024. Panel (d) is reproduced from ref. 41 with permission from American Chemical Society, copyright 2016.

lipoproteins, macrophages, and inflammatory mediators within the coronary arterial intima. Without timely intervention, CHD progresses towards luminal stenosis and myocardial hypoperfusion, and eventually acute myocardial infarction and heart failure.<sup>106</sup> Thus, early diagnosis and continuous monitoring of

CHD progression are crucial strategies to prevent the development of life-threatening cardiovascular events. Hydrogen sulfide (H<sub>2</sub>S) is a gaseous signaling molecule in blood that can hardly be quantified by traditional blood analysis methods because of its low concentration and unstable nature.<sup>107</sup> Clinical studies

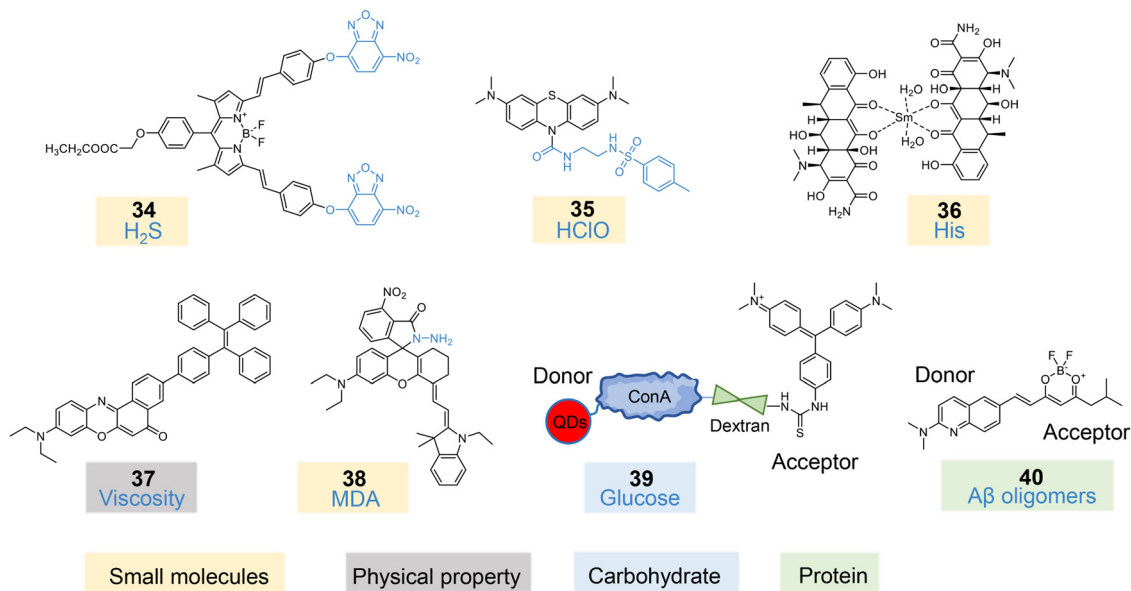


**Fig. 11** Chemical structures of AOPs **34–40** for other disease diagnostics in blood (AOPs **34–37**), urine (AOP **38**), tear (AOP **39**), and cerebrospinal fluid (AOP **40**). H<sub>2</sub>S, hydrogen sulfide; HClO, hypochlorous acid; His, histidine; MDA, malondialdehyde; A $\beta$  oligomers, amyloid-beta oligomers.



showed that an abnormally low  $\text{H}_2\text{S}$  concentration is consistently reported in cardiovascular patients.<sup>108</sup> Moreover, the strong autofluorescence of blood poses a significant challenge for fluorescence-based assays, particularly for quantifying trace components. To tackle these challenges, Yang *et al.* reported AOP 34 based on a BODIPY dye that quenches blood autofluorescence through the inner filter effect and fluoresces in the presence of  $\text{H}_2\text{S}$  with a LOD value of 28.0 nM (Fig. 11).<sup>42</sup> In the AOP 34-based blood test, the endogenous blood  $\text{H}_2\text{S}$  was quantified in 20-fold diluted whole blood samples within 30–50 minutes. AOP 34 also successfully distinguished blood samples

of CHD patients from those of healthy individuals, and the results were consistent with clinical ELISA measurements (Fig. 12a and b). Therefore, AOP 34 offers a promising tool for early CHD diagnosis through the advantages of whole blood analysis, enhanced sensitivity, simpler, faster, and more cost-effective operation.

Diabetes mellitus is a chronic metabolic disorder affecting millions of people worldwide.<sup>109</sup> Early diagnosis and continuous monitoring of blood glucose levels are crucial for effective management of diabetes and preventing complications. In diabetes pathophysiology, abnormally high reactive oxygen

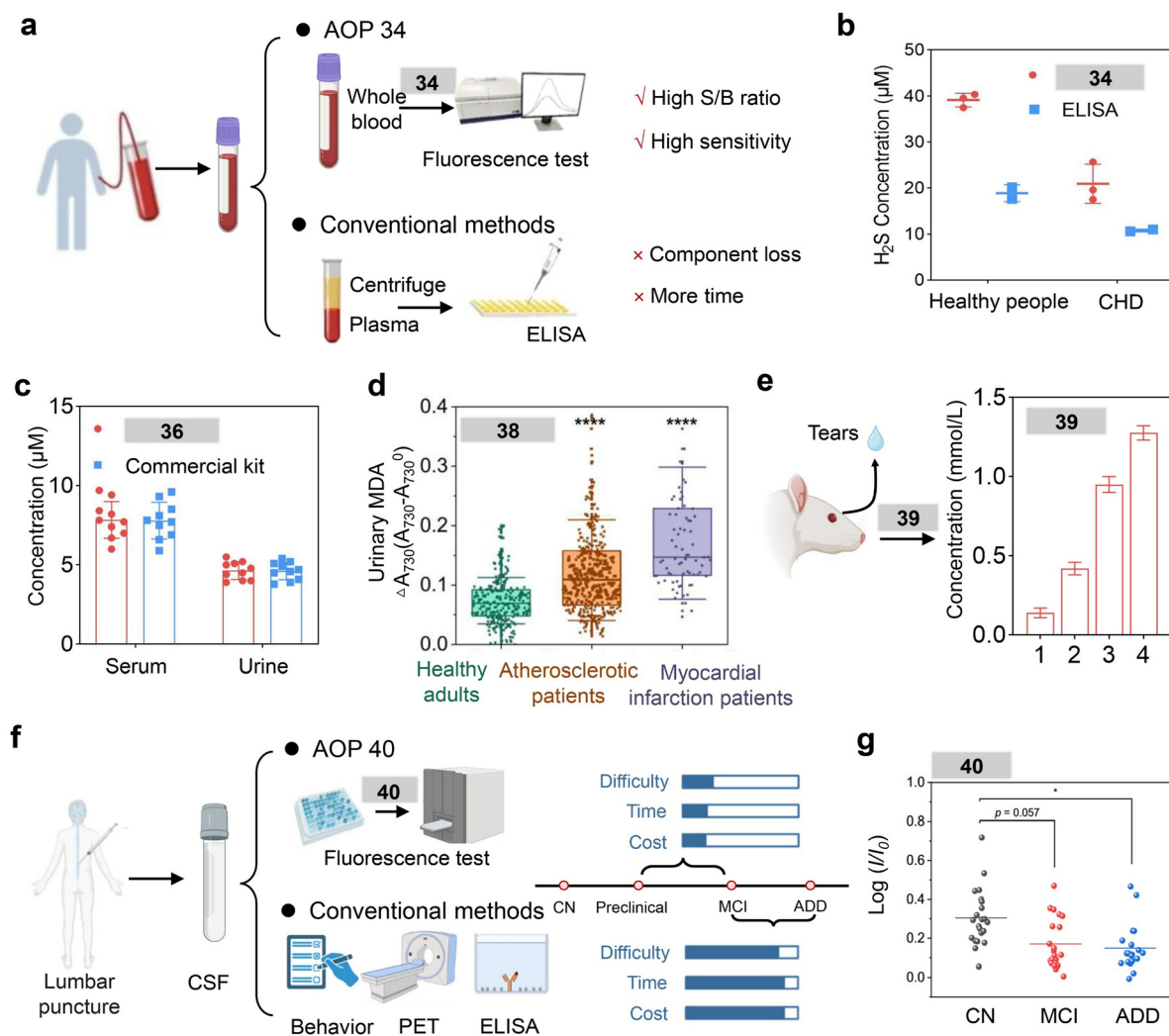


**Fig. 12** Other disease diagnostics using AOPs. (a) Workflow comparison between AOP 34-based blood analysis and the conventional ELISA method. (b) Quantitative comparison of  $\text{H}_2\text{S}$  detection between AOP 34 and ELISA in healthy people and CHD patients (mean  $\pm$  s.d.,  $n = 3$ ). CHD, coronary heart disease. (c) Comparative analysis of histidine levels in the serum and urine samples from histidinemia patients using AOP 36 versus the commercial kit. (d) Urinary MDA levels among healthy controls, atherosclerotic patients, and myocardial infarction patients using AOP 38 (\*\*\*\* $p < 0.0001$ ,  $n = 265$  for healthy controls,  $n = 374$  for atherosclerotic patients,  $n = 76$  for myocardial infarction patients). (e) Quantitative analysis of tear glucose levels in 4 individual rats using AOP 39. (f) Workflow comparison between AOP 40-based CSF analysis and conventional AD diagnostic methods (behavioral tests, PET imaging, and ELISA). (g) Fluorescence intensity ratio of CSF samples using AOP 40 across three groups: CN,  $n = 22$ , MCI,  $n = 21$ , and ADD,  $n = 18$ . CSF, cerebrospinal fluid; PET, positron emission tomography; ELISA, enzyme-linked immunosorbent assay; CN, cognitive normal; MCI, mild cognitive impairment; ADD, Alzheimer's disease dementia. \* $p < 0.05$ . Panels (a) and (b) are reproduced from ref. 42 with permission from Wiley-VCH GmbH, copyright 2023. Panel (c) is reproduced from ref. 44 with permission from Elsevier B.V., copyright 2017. Panel (d) is reproduced from ref. 46 with permission from the authors, copyright 2023. Panel (e) is reproduced from ref. 47 with permission from Elsevier B.V., copyright 2017. Panels (f) and (g) are reproduced from ref. 48 with permission from the authors, copyright 2024.



species are produced due to the oxidative glucose phosphorylation. In particular, overexpression of hypochlorous acid (HClO) is related to vascular endothelial dysfunction, cell death, and ultimately causes diabetes development.<sup>110</sup> He and coworkers reported AOP 35 based on an NIR fluorescent probe consisting of methylene blue and a methyl sulfonamide moiety (Fig. 11).<sup>43</sup> AOP 35 showed a 45-fold NIR fluorescence enhancement after HClO oxidization, followed by amide bond cleavage. AOP 35 presented high detection sensitivity towards HClO with a LOD value of 0.29  $\mu\text{M}$  and a rapid response time of 2 seconds. In the AOP 35-based serum test, approximately 7-fold fluorescence enhancement was observed in the diabetic patients' serum as compared to serum from healthy controls.

Histidinemia is a rare hereditary metabolic disorder characterized by deficiency of enzyme histidase, which is necessary for the metabolism of the amino acid histidine. This condition results in elevated blood histidine levels from normal (70–120  $\mu\text{M}$ ) to high levels (290–1420  $\mu\text{M}$ ), potentially leading to developmental issues in affected children. Attia *et al.* introduced AOP 36 (Fig. 11), a samarium-tetracycline complex doped in the sol-gel matrix, for early diagnosis of histidinemia in newborn children.<sup>44</sup> AOP 36 exhibits enhanced luminescence at 645 nm when histidine replaces water molecules in the coordination sphere of the Sm complex through electrostatic attraction between the positive charge of the complex and the negative charge of histidine at pH 9.2. AOP 36 exhibited high detection sensitivity and selectivity towards histidine, with a linear signal response to histidine concentrations from  $1.4 \times 10^{-5}$  to  $6.5 \times 10^{-10}$  mol L<sup>-1</sup> and a LOD value of  $3.2 \times 10^{-10}$  mol L<sup>-1</sup>. AOP 36 was then applied to detect histidine in the clinical serum and urine samples of Histidinemia disease, and achieved high diagnostic sensitivity (98.88%) and specificity (97.41%) (Fig. 12c). Besides, AOP 36-based body fluid diagnostics showed consistent results with clinical standard methods. Therefore, AOP 36 presented a promising approach for the early, accurate, and convenient diagnosis of histidinemia in newborns.

Folliculitis and peritonitis represent two distinct types of inflammatory conditions – localized skin inflammation and systemic abdominal inflammation.<sup>111</sup> Blood viscosity serves as a crucial biomarker for inflammatory conditions, as inflammation can alter blood rheological properties through changes in the plasma protein composition and cellular components.<sup>112</sup> Lin and coworkers designed AOP 37 for detection of blood viscosity, combining Nile red as the acceptor and tetraphenylethylene (TPE) as the donor based on TBET (Fig. 11).<sup>45</sup> AOP 37 showed ratiometric responses (460 nm/675 nm) with enhanced viscosity, with a 231-fold increase in fluorescence intensity ratio ( $I_{460}/I_{675}$ ) over a wide viscosity range (1.40 to 953 cp). In preclinical blood samples of folliculitis and peritonitis mouse models, AOP 37 successfully detected increased blood viscosity (1.51-fold in folliculitis and 1.21–1.27-fold in peritonitis) with minimal sample requirement (10  $\mu\text{L}$  blood).

**3.5.2. Urine.** Atherosclerosis plays a key role in cardiovascular diseases, creating an urgent need for early detection and monitoring strategies.<sup>113</sup> Both chronic and acute inflammation of vascular walls can cause increased systemic oxidative stress,

which significantly contributes to the development of atherosclerosis.<sup>114</sup> Among various biomarkers, malondialdehyde (MDA) stands out as a stable oxidative stress indicator that can be detected in urine, making urinary MDA a promising biomarker for systemic oxidative stress assessment in atherosclerosis. Zhang's group designed a near-infrared MDA-responsive molecule (AOP 38) based on PET and ICT mechanisms (Fig. 11).<sup>46</sup> AOP 38 detected urinary MDA detection with a LOD value of 163 nM in only 10  $\mu\text{L}$  of urine sample and 30 minutes processing time. In a large-scale clinical validation study involving more than 600 participants, AOP 38 showed that the urinary MDA levels were higher in atherosclerotic patients (1.71-fold) and myocardial infarction patients (2.56-fold) than those in healthy adults (Fig. 12d).

**3.5.3. Tear fluid.** Tear fluid, with its non-invasive collection process and rich biochemical composition, serves as an accessible and valuable diagnostic medium.<sup>115</sup> Researchers had shown that tear glucose levels are about 5 times higher in diabetics than in healthy controls. Compared to traditional clinical methods for diabetes detection, including finger-prick blood tests and continuous glucose monitors, often leading to poor patient compliance due to discomfort and the need for frequent testing, tear-based glucose detection offers a promising alternative for atraumatic and patient-friendly diabetes management. Zhang's group developed AOP 39 that is constructed by conjugating CdSe/ZnS quantum dots (QDs), dextran-bound malachite green (MG), and concanavalin A as the FRET donor, acceptor and glucose active-targeting agent, respectively (Fig. 11).<sup>47</sup> The QDs' fluorescence is quenched by MG through FRET but restored in the presence of glucose through competitive binding. Upon glucose incubation, AOP 39 showed signal activation with a linear response to glucose concentrations (0.03 to 3 mmol L<sup>-1</sup>), covering the range of tear glucose levels for both diabetics ( $0.35 \pm 0.04$  mmol L<sup>-1</sup>) and healthy people ( $0.16 \pm 0.03$  mmol L<sup>-1</sup>). In the preclinical test, AOP 39 successfully detected glucose levels in 2  $\mu\text{L}$  of tear samples within 30 seconds in a diabetic rat model (Fig. 12e).

**3.5.4. Cerebrospinal fluid.** Cerebrospinal fluid (CSF), with its direct contact with neural tissues and relatively simple matrix composition, offers a promising diagnostic medium in central nervous system pathologies. Given its unique anatomical location and continuous exchange with brain interstitial fluid, CSF provides critical insights into neurodegenerative processes, such as Alzheimer's disease (AD), meningitis, multiple sclerosis and glioblastoma.<sup>116</sup> Among these, AD is a kind of neurodegenerative disorder, affecting millions of individuals worldwide and posing a significant global health challenge.<sup>117</sup> Current clinical diagnostic approaches, including behavioral assessments, PET imaging, and ELISA, have limitations such as specialized instrumentations, prolonged detection time, and high cost (Fig. 12f). AOPs have shown potential in detecting neurodegenerative biomarkers with high sensitivity and specificity, enabling real-time monitoring of disease progression and therapeutic response. The presence of amyloid- $\beta$  ( $\text{A}\beta$ ) species, particularly soluble  $\text{A}\beta$  oligomers, in CSF represents potential early-stage biomarkers for AD, as these molecules play fundamental roles in disease pathogenesis and cognitive decline.



Based on these, Kim and coworkers developed AOP **40**, a donor- $\pi$ -acceptor fluorescent probe consisting of N,N-dimethylquinoline and dioxaborine-based half-curcumin, for the selective detection of A $\beta$  oligomers in AD (Fig. 11).<sup>48</sup> AOP **40** exhibited enhanced fluorescence upon binding to hydrophobic regions of A $\beta$  oligomers, with a LOD value of  $0.57 \pm 0.04$  nM. In clinical applications using CSF samples, AOP **40**-based body fluid diagnostics successfully distinguished between cognitive normal ( $\log(I/I_0) = 0.34 \pm 0.13$ ), mild cognitive impairment ( $0.15 \pm 0.12$ ), and AD dementia ( $0.14 \pm 0.10$ ) states (Fig. 12g). As compared to the traditional thioflavin T-based staining method or antibody-based ELISA methods, AOP **40**-based body fluid diagnostics offered advantages including higher detection selectivity, simpler operational protocols, and more cost-effective procedures. Therefore, AOP **40** represents a significant advancement in AD research and diagnosis, as it provides a sensitive and selective tool for detecting A $\beta$  oligomers across various biological samples and applications. The application of AOPs in neurodegenerative disease detection offers significant advantages, including early diagnosis capability, friendly operation procedures, and cost-effectiveness, making it a promising tool for routine clinical applications.

## 4. Summary and outlook

The past decade has witnessed the development of AOP-based body fluid diagnostics in both preclinical and clinical applications. With high detection sensitivity and specificity towards biomarkers-of-interest, AOP-based body fluid diagnostics could detect biomarkers at extreme low concentrations in the intricate body fluid (for example, AOP **30** achieved LOD values of 0.249 and  $0.877 \text{ U L}^{-1}$  for MAO and LAP, respectively) and, therefore, diagnose diseases at an early stage. Additionally, with high detection sensitivity, AOP-based body fluid diagnostics only require minimal sample volumes, as demonstrated by AOP **39** that could detect glucose in just  $2 \mu\text{L}$  of tear fluids, making them particularly valuable in analyses of precious or hard-to-obtain fluids like the cerebrospinal fluid. Besides, by virtue of the direct, quick chemical response of AOP towards biomarkers, AOP-based body fluid diagnostics typically requires short measurement times with systems like AOP **22** capable of recognizing BlaC within 10 min and eliminates the need for complicated instrumentations and well-trained technicians. Together, these properties endow AOPs a valuable tool for primary healthcare providers and even patients at home in the POCT settings.

Despite the significant progress achieved, AOP-based body fluid diagnostics still faces challenges in both limited molecular design approaches and applications. Firstly, most AOPs are designed for single biomarker detection, yet simultaneous detection of multiple biomarkers is typically required for accurate and comprehensive disease assessments. Multiplex detection with several AOPs requires careful molecular designs to avoid optical signal crosstalk. However, only limited multi-lock AOPs, which allow simultaneous detection of multiple biomarkers (for example, AOPs **29**, **30** and **31**), have been

reported for body fluid diagnostics. Secondly, the complex compositions in body fluids, such as red blood cells, proteins, and electrolytes, can interfere with signal readouts and pose challenges on the optical properties of AOPs. To resolve this issue, AOP **34** has been developed based on a BODIPY dye that quenches blood autofluorescence through an inner filter effect, and detected the presence of H<sub>2</sub>S in blood with a LOD value of 28.0 nM. However, novel approaches to reduce the background signal interference from body fluids are still lacking. Thirdly, from the application perspective, the optical signal stability and degradation behaviors of AOPs remain undiscovered, which could potentially compromise the stability and reliability of AOP-based body fluid diagnostics. Moreover, it is necessary to expand the application of AOPs to more body fluids to assist clinical diagnosis and treatment evaluation. Different body fluids achieve diagnostic needs for various diseases. For instance, the lymphatic fluid is crucial for monitoring cancer metastasis and immune responses, the peritoneal fluid provides insights into abdominal pathologies, and the amniotic fluid offers critical information for prenatal diagnostics.

To tackle these challenges, the AOP design and detection methodologies could be potentially improved in the following directions. Firstly, AOPs responsive towards multiple biomarkers could be developed to improve the disease diagnostic accuracy. This relies on careful biomarker selection through integrated multi-omics technologies and designing sophisticated responsive optical signal transitions with cost-effective synthesis strategies. Secondly, AOP-based body fluid diagnostics could be incorporated into high-throughput detection systems (for example, microfluidic techniques) to achieve rapid and parallel sample processing. With the advantages of simple operations and direct signal readouts, AOP-based body fluid diagnostics could also be incorporated into POCT or wearable devices. Furthermore, the integration of artificial intelligence (AI) into AOP design in body fluid diagnostics offers optimization approaches beyond traditional empirical methods. AI-driven virtual screening efficiently identifies promising molecular candidates from chemical libraries, while machine learning models analyze structure–activity relationships to guide rational probe design, optimizing sensitivity, selectivity, and activation efficiency. Advanced AI algorithms can simultaneously balance multiple performance metrics, including fluorescence intensity, stability, biocompatibility, and even simulate the pathophysiologic conditions especially for the hard-to-obtain body fluid samples. Moreover, by integrating multi-omics data, AI can guide the design of multi-responsive AOPs with minimal signal crosstalk. This interdisciplinary collaboration among computational scientists, chemists, biologists, and clinical researchers, leading to robust high-quality databases and advanced model training systems, accelerates the development of next-generation AOPs for body fluid diagnostics.

## Glossary

AAP	Alanine aminopeptidase
A $\beta$	Amyloid- $\beta$
AD	Alzheimer's disease



Ag85	Antigen 85
AIE	Aggregation-induced emission
ALB	Albumin
AMY	$\alpha$ -Amylase
AO	Auramine O
AOPs	Activatable optical probes
APN	Aminopeptidase N
BlaC	$\beta$ -Lactamase
BUN	Blood urea nitrogen
Cas-1	Caspase-1
CHD	Coronary heart disease
CLIA	Chemiluminescence immunoassay
CSF	Cerebrospinal fluid
CTCs	Circulating tumor cells
Cys	Cysteine
DIKI	Drug-induced kidney injury
dPCR	Digital polymerase chain reaction
DPP-IV	Dipeptidyl peptidase-IV
ELISA	Enzyme-linked immunosorbent assay
ESBL/AmpC	Extended-spectrum/AmpC $\beta$ -lactamases
FRET	Förster resonance energy transfer
GBM	Glioblastoma
GC-MS	Gas chromatography–mass spectrometry
GFR	Glomerular filtration rate
GGT	$\gamma$ -Glutamyl transpeptidase
HClO	Hypochlorous acid
Hcy	Homocysteine
His	Histidine
H <sub>2</sub> O <sub>2</sub>	Hydrogen peroxide
H <sub>2</sub> S	Hydrogen sulfide
HSA	Human serum albumin
HSP	Heat shock protein
ICT	Intramolecular charge transfer
IVD	<i>In vitro</i> diagnostics
LAP	Leucine aminopeptidase
LOD	Limit-of-detection
LPS	Lipase
mALB	Microalbumin
MAO	Monoamine oxidase
MDA	Malondialdehyde
MG	Malachite green
<i>Mtb</i>	<i>Mycobacterium tuberculosis</i>
NAG	<i>N</i> -acetyl- $\beta$ - <i>D</i> -glucosaminidase
NO	Nitric oxide
NR	Not reported
NSET	Nanomaterials-based surface energy transfer
PET	Photoinduced electron transfer
PCR	Polymerase chain reaction
POC	Point-of-care
POCT	Point-of-care testing
POPF	Postoperative pancreatic fistula
QDs	Quantum dots
qPCR	Quantitative real-time polymerase chain reaction
ROC	Receiver operating characteristic
RT-PCR	Reverse transcription–polymerase chain reaction
Rv3368c	Nitroreductase Rv3368c

<i>S. aureus</i>	<i>Staphylococcus aureus</i>
SBRs	Signal-to-background ratios
SCr	Serum creatinine
sLeX	Sialyl Lewis X
TBET	Through bond energy transfer
TICT	Twisted intramolecular charge transfer
TPE	Tetraphenylethylene
UA	Uric acid

## Data availability

No primary research results, software or code have been included and no new data were generated or analysed as part of this review.

## Conflicts of interest

The authors declare no conflicts of interest.

## Acknowledgements

J. Z. thanks the National Natural Science Foundation of China (32101058), the Guangdong Basic and Applied Basic Research Foundation (2023A1515012734), and the Outstanding Youths Development Scheme of Nanfang Hospital, Southern Medical University (2023J006); L. Z. thanks the National Science Fund for Distinguished Young Scholars (82025024); K. P. thanks the Singapore National Research Foundation (NRF) (NRF-NRF107-2021-0005), and the Singapore Ministry of Education, Academic Research Fund Tier 2 (MOE-T2EP30220-0010; MOE-T2EP30221-0004) for the financial support.

## References

- 1 E. Cooke, Presented in part at the Selection And Use Of Essential *In Vitro* Diagnostics: Report Of the Second Meeting Of the Who Strategic Advisory Group Of Experts on *In Vitro* Diagnostics, 2019 (Including the Second Who Model List Of Essential In Vitro Diagnostics), 2019.
- 2 J. Heikenfeld, A. Jajack, B. Feldman, S. W. Granger, S. Gaitonde, G. Begtrup and B. A. Katchman, *Nat. Biotechnol.*, 2019, **37**, 407–419.
- 3 K. J. Land, D. I. Boeras, X. S. Chen, A. R. Ramsay and R. W. Peeling, *Nat. Microbiol.*, 2019, **4**, 46–54.
- 4 N. S. I. S. Team, *Regulatory Knowledge Guide for In Vitro Diagnostics*, 2023.
- 5 A. Barhoum, Z. Altintas, K. S. S. Devi and R. J. Förster, *Nano Today*, 2023, **50**, 101874.
- 6 M. Clarke and M. Marzinke, *Contemporary Practice in Clinical Chemistry*, 2020.
- 7 P. H. Cheng and K. Y. Pu, *Chem. Soc. Rev.*, 2024, **53**, 10171–10188.
- 8 L. L. Wu, J. G. Huang, K. Y. Pu and T. D. James, *Nat. Rev. Chem.*, 2021, **5**, 406–421.



- 9 X. Wu, R. Wang, N. Kwon, H. Ma and J. Yoon, *Chem. Soc. Rev.*, 2022, **51**, 450–463.
- 10 R. R. Nair, J. M. An, J. Kim and D. Kim, *Coord. Chem. Rev.*, 2023, **494**, 215336.
- 11 C. Xu and K. Y. Pu, *Nat. Rev. Bioeng.*, 2024, **2**, 425–441.
- 12 H. X. Xie, J. Mire, Y. Kong, M. Chang, H. A. Hassounah, C. N. Thornton, J. C. Sacchettini, J. D. Cirillo and J. H. Rao, *Nat. Chem.*, 2012, **4**, 802–809.
- 13 Z. Zhu, X. Chen, H. Liao, L. Li, H. Yang, Q. Wang and W. H. Zhu, *Aggregate*, 2024, **5**, e526.
- 14 J. Ou-Yang, Y. Li, W. L. Jiang, S. Y. He, H. W. Liu and C. Y. Li, *Anal. Chem.*, 2019, **91**, 1056–1063.
- 15 S. Li, R. Hu, C. Yang, X. Zhang, Y. Zeng, S. Wang, X. Guo, Y. Li, X. Cai, S. Li, C. Han and G. Yang, *Biosens. Bioelectron.*, 2017, **98**, 325–329.
- 16 Y. Kim, J. M. An, J. Kim, T. Chowdhury, H. J. Yu, K. M. Kim, H. Kang, C. K. Park, J. F. Joung, S. Park and D. Kim, *Anal. Chim. Acta*, 2022, **1202**, 339678.
- 17 C. Li, R. Pan, P. Li, Q. Guan, J. Ao, K. Wang, L. Xu, X. Liang, X. Jin, C. Zhang and X. Zhu, *Anal. Chem.*, 2017, **89**, 5966–5975.
- 18 J. Huang, Y. Jiang, J. Li, S. He, J. Huang and K. Pu, *Angew. Chem., Int. Ed.*, 2020, **59**, 4415–4420.
- 19 J. M. An, J. Suh, J. Kim, Y. Kim, J. Y. Chung, H. S. Kim, S. Y. Cho, J. H. Ku, C. Kwak, H. H. Kim, C. W. Jeong and D. Kim, *Sens. Actuators, B*, 2022, **360**, 131646.
- 20 J. M. An, M. Jeong, J. Jung, S. G. Yeo, S. Park and D. Kim, *ACS Appl. Mater. Interfaces*, 2024, **16**, 4493–4504.
- 21 C. Wang, X. Wang, J. Lu, D. Wei, N. Zhou, Y. Li, Y. Wang and H. Z. He, *Sens. Actuators, B*, 2023, **392**, 134040.
- 22 S. Jiao, S. Yang, Y. Y. Wang and A. Ma, *Sens. Actuators, B*, 2023, **374**, 132790.
- 23 J. Jongkhumkrong, I. Thaveesangsakulthai, W. Sukbangnop, C. Kulsing, T. Sooksimuang, C. Aonbangkhen, S. Sahasithiwat, T. Sriprasart, T. Palaga, N. Chantaravisoot and B. Tomapatanaget, *ACS Appl. Mater. Interfaces*, 2022, **14**, 49495–49507.
- 24 J. Huang, J. Li, Y. Lyu, Q. Miao and K. Pu, *Nat. Mater.*, 2019, **18**, 1133–1143.
- 25 P. Cheng, Q. Miao, J. Huang, J. Li and K. Pu, *Anal. Chem.*, 2020, **92**, 6166–6172.
- 26 K. Yamada, T. Takata, T. Iyama, S. Hamada, Y. Mae, T. Sugihara and H. Isomoto, *Int. J. Mol. Sci.*, 2022, **23**, 8150.
- 27 S. Sarkar, A. Shil, Y. L. Jung, S. Singha and K. H. Ahn, *ACS Sens.*, 2022, **7**, 3790–3799.
- 28 H. Wang, J. Wang, G. Ma, J. Zhou, L. Du, H. Wu, X. Zhang, Y. He and J. Zhou, *Chem. Eng. J.*, 2023, **464**, 142551.
- 29 Y. Tu, Y. Yu, Z. Zhou, S. Xie, B. Yao, S. Guan, B. Situ, Y. Liu, R. T. K. Kwok, J. W. Y. Lam, S. Chen, X. Huang, Z. Zeng and B. Z. Tang, *ACS Appl. Mater. Interfaces*, 2019, **11**, 29619–29629.
- 30 H. Xu, G. Shen, C. Peng, X. Han, L. Duan and T. Cheng, *Dyes Pigm.*, 2022, **197**, 109915.
- 31 X. Hong, P. Geng, N. Tian, X. Li, M. Gao, L. Nie, Z. Sun and G. Liu, *Anal. Chem.*, 2024, **96**, 1576–1586.
- 32 Y. F. Cheng, J. H. Xie, K. H. Lee, R. L. Gaur, A. G. Song, T. T. Dai, H. J. Ren, J. N. Wu, Z. G. Sun, N. Banaei, D. Akin and J. H. Rao, *Sci. Transl. Med.*, 2018, eaar4470.
- 33 M. Kamariza, P. Shieh, C. S. Ealand, J. S. Peters, B. Chu, F. P. Frances, P. Rodriguez-Rivera, M. R. B. Sait, W. V. Treuren, N. Martinson, R. Kalscheuer, B. D. Kana and C. R. Bertozzi, *Sci. Transl. Med.*, 2018, **10**, eaam6310.
- 34 J. W. A. Schoenmakers, M. Lopez-Alvarez, I. J. FFA, M. Wouthuyzen-Bakker, J. O. McNamara, 2nd, M. van Oosten, P. C. Jutte and J. M. van Dijn, *Eur. J. Nucl. Med. Mol. Imaging*, 2024, **51**, 2988–2997.
- 35 Y. Yang, M. Wu, Y. Zhang, L. Wang, Y. Song, H. Xiao and E. Song, *Chem. Eng. J.*, 2024, **485**, 149539.
- 36 G. Liu, W. Li, S. Li, J. Xu, X. Wang, H. Xu, D. Liu and H. Gao, *Biosens. Bioelectron.*, 2024, **257**, 116300.
- 37 Y. Liu, L. Teng, C. Xu, H. W. Liu, S. Xu, H. Guo, L. Yuan and X. B. Zhang, *Chem. Sci.*, 2019, **10**, 10931–10936.
- 38 M. Chen, C. Wang, Z. Ding, H. Wang, Y. Wang and Z. Liu, *ACS Cent. Sci.*, 2022, **8**, 837–844.
- 39 J. Shi, Q. Deng, Y. Li, Z. Zheng, H. Shangguan, L. Li, F. Huang and B. Tang, *Chem. Commun.*, 2019, **55**, 6417–6420.
- 40 J. Shi, Q. Deng, Y. Li, M. Zheng, Z. Chai, C. Wan, Z. Zheng, L. Li, F. Huang and B. Tang, *Anal. Chem.*, 2018, **90**, 13775–13782.
- 41 N. Hamano, M. Murata, T. Kawano, J. S. Piao, S. Narahara, R. Nakata, T. Akahoshi, T. Ikeda and M. Hashizume, *ACS Appl. Mater. Interfaces*, 2016, **8**, 5114–5123.
- 42 Z. Yuwen, Q. Zeng, Q. Ye, Y. Zhao, J. Zhu, K. Chen, H. Liu and R. Yang, *Angew. Chem. Int. Ed.*, 2023, **62**, e202302957.
- 43 S. Li, K. Yang, Y. Liu, P. Wang, D. Cheng and L. He, *Sens. Actuators, B*, 2023, **379**, 133253.
- 44 M. S. Attia, *Biosens. Bioelectron.*, 2017, **94**, 81–86.
- 45 O. Raitakari, K. Pakkala and C. G. Magnussen, *Nat. Rev. Cardiol.*, 2022, **19**, 543–554.
- 46 Y. Ma, W. Sun, Z. F. Ye, L. H. Liu, M. H. Li, J. H. Shang, X. Y. Xu, H. Cao, L. Xu, Y. C. Liu, X. Q. Kong, G. S. Song and X. B. Zhang, *Sci. Adv.*, 2023, **9**, eadh1037.
- 47 L. Chen, W. H. Tse, Y. Chen, M. W. McDonald, J. Melling and J. Zhang, *Biosens. Bioelectron.*, 2017, **91**, 393–399.
- 48 J. An, K. Kim, H. J. Lim, H. Y. Kim, J. Shin, I. Park, I. Cho, H. Y. Kim, S. Kim, C. McLean, K. Y. Choi, Y. Kim, K. H. Lee and J. S. Kim, *Nat. Commun.*, 2024, **15**, 1004.
- 49 C. Li, S. Zhou, J. Chen and X. Jiang, *Chem. Biomed. Imaging*, 2023, **1**, 495–508.
- 50 S. Y. Liu, A. M. Yan, W. Y. Guo, Y. Y. Fang, Q. J. Dong, R. R. Li, S. N. Ni, Y. Sun, W. C. Yang and G. F. Yang, *ACS Nano*, 2020, **14**, 4244–4254.
- 51 R. Vankayala and K. C. Hwang, *Adv. Mater.*, 2018, **30**, e1706320.
- 52 J. Kramer, R. Kang, L. M. Grimm, L. De Cola, P. Picchetti and F. Biedermann, *Chem. Rev.*, 2022, **122**, 3459–3636.
- 53 D. Liang, Y. Wang and K. Qian, *Interdiscip. Med.*, 2023, **1**, e20230020.
- 54 Q. Wang, S. Yang, F. Li and D. Ling, *Interdiscip. Med.*, 2023, **1**, e20220004.
- 55 S. Lee, E. Kim, C. E. Moon, C. Park, J. W. Lim, M. Baek, M. K. Shin, J. Ki, H. Cho, Y. W. Ji and S. Haam, *Nat. Commun.*, 2023, **14**, 8153.
- 56 Y. X. Hu, J. Yu, M. K. Xu and K. Y. Pu, *J. Am. Chem. Soc.*, 2024, **146**, 12656–12663.



- 57 C. R. Hoopes, F. J. Garcia, A. M. Sarkar, N. J. Kuehl, D. T. Barkan, N. L. Collins, G. E. Meister, T. R. Bramhall, C. H. Hsu, M. D. Jones, M. Schirle and M. T. Taylor, *J. Am. Chem. Soc.*, 2022, **144**, 6227–6236.
- 58 J. Ouyang, L. H. Sun, F. Zeng and S. Z. Wu, *Coord. Chem. Rev.*, 2022, **458**, 214438.
- 59 Z. R. Zhu, Q. Wang, X. Y. Chen, Q. Wang, C. X. Yan, X. L. Zhao, W. J. Zhao and W. H. Zhu, *Adv. Mater.*, 2022, **34**, 2107444.
- 60 C. Yan, Z. Zhu, Y. Yao, Q. Wang, Z. Guo and W.-H. Zhu, *Acc. Mater. Res.*, 2024, **5**, 64–75.
- 61 A. R. Sekhar, Y. Chitose, J. Janos, S. I. Dangoor, A. Ramundo, R. Satchi-Fainaro, P. Slavíček, P. Klan and R. Weinstain, *Nat. Commun.*, 2022, **13**, 3614.
- 62 B. H. Li, H. K. Liu, Y. L. He, M. Y. Zhao, C. Ge, M. R. Younis, P. Huang, X. Y. Chen and J. Lin, *Angew. Chem., Int. Ed.*, 2022, **61**, e202200025.
- 63 B. Valeur and M. N. Berberan-Santos, *Molecular Fluorescence: Principles and Applications*, 2012.
- 64 E. A. Jares-Erijman and T. M. Jovin, *Nat. Biotechnol.*, 2003, **21**, 1387–1395.
- 65 Y. Hong, J. W. Y. Lam and B. Z. Tang, *Chem. Soc. Rev.*, 2011, **40**, 5361–5388.
- 66 R. L. Siegel, A. N. Giaquinto and A. Jemal, *Ca-Cancer J. Clin.*, 2024, **74**, 203.
- 67 S. N. Lone, S. Nisar, T. Masoodi, M. Singh, A. Rizwan, S. Hashem, W. El-Rifai, D. Bedognetti, S. K. Batra, M. Haris, A. A. Bhat and M. A. Macha, *Mol. Cancer*, 2022, **21**, 79.
- 68 B. L. Wang, S. Q. Hu, Y. Teng, J. L. Chen, H. Y. Wang, Y. Z. Xu, K. Y. Wang, J. G. Xu, Y. Z. Cheng and X. Gao, *Signal Transduction Targeted Ther.*, 2024, **9**, 200.
- 69 M. Touray and A. Touray, *Clinical Work and General Management of a Standard Minimal-Resource Facility*, 2021.
- 70 Y. Zhou, L. Tao, J. H. Qiu, J. Xu, X. Y. Yang, Y. Zhang, X. Y. Tian, X. Q. Guan, X. B. Cen and Y. L. Zhao, *Signal Transduction Targeted Ther.*, 2024, **9**, 132.
- 71 L. W. Ma, H. L. Guo, Y. X. Zhao, Z. B. Liu, C. R. Wang, J. H. Bu, T. Sun and J. W. Wei, *Signal Transduction Targeted Ther.*, 2024, **9**, 336.
- 72 H. Yan, H. Ma, B. He, B. Yu, Y. Q. Shen and H. L. Cong, *Nano Res.*, 2023, **16**, 7075–7084.
- 73 C. Grimm, G. Hofstetter, S. Aust, I. Mutz-Dehbalaie, M. Bruch, G. Heinze, J. Rahhal-Schupp, A. Reinthaller, N. Concin and S. Polterauer, *Br. J. Cancer*, 2013, **109**, 610–614.
- 74 J. Lin, I. M. Lee, Y. Q. Song, N. R. Cook, J. Selhub, J. E. Manson, J. E. Buring and S. M. Zhang, *Cancer Res.*, 2010, **70**, 2397–2405.
- 75 M. Maas, T. Todenhöfer and P. C. Black, *Nat. Rev. Urol.*, 2023, **20**, 597–614.
- 76 L. Guzman-Rojas, R. Rangel, A. Salameh, J. K. Edwards, E. Dondossola, Y. G. Kim, A. Saghatelian, R. J. Giordano, M. G. Kolonin, F. I. Staquicini, E. Koivunen, R. L. Sidman, W. Arap and R. Pasqualini, *Proc. Natl. Acad. Sci. U. S. A.*, 2012, **109**, 1637–1642.
- 77 T. W. Rockett, M. Almahyawi, M. L. Ghimire, A. Jonnalagadda, V. Tagliaferro, S. J. Seashols-Williams, M. F. Bertino, G. A. Caputo and J. E. Reiner, *ACS Sens.*, 2024, **9**, 860–869.
- 78 S. R. Barthel, G. K. Wiese, J. H. Cho, M. J. Opperman, D. L. Hays, J. Siddiqui, K. J. Pienta, B. Furie and C. J. Dimitroff, *Proc. Natl. Acad. Sci. U. S. A.*, 2009, **106**, 19491–19496.
- 79 Y. Zhang, J. Sun, C. C. Lin, E. Abemayor, M. B. Wang and D. T. W. Wong, *Periodontology 2000*, 2016, **70**, 38–52.
- 80 M. Arif, B. M. Vedamurthy, R. Choudhari, Y. B. Ostwal, K. Mantelingu, G. S. Kodaganur and T. K. Kundu, *Chem. Biol.*, 2010, **17**, 903–913.
- 81 W. T. Liu, Y. P. Cao, X. H. Zhou and D. Han, *Adv. Sci.*, 2022, **9**, 2100617.
- 82 M. Friedel, I. A. P. Thompson, G. Kasting, R. Polsky, D. Cunningham, H. T. Soh and J. Heikenfeld, *Nat. Biomed. Eng.*, 2023, **7**, 1541–1555.
- 83 M. Hakim, Y. Y. Broza, O. Barash, N. Peled, M. Phillips, A. Amann and H. Haick, *Chem. Rev.*, 2012, **112**, 5949–5966.
- 84 A. B. Sanz, M. D. Sanchez-Nino, A. M. Ramos and A. Ortiz, *Nat. Rev. Nephrol.*, 2023, **19**, 281–299.
- 85 S. L. Wood, M. A. Knowles, D. Thompson, P. J. Selby and R. E. Banks, *Nat. Rev. Urol.*, 2013, **10**, 206–218.
- 86 B. Thomas and D. Tolley, *Nat. Clin. Pract. Urol.*, 2008, **5**, 668–675.
- 87 M. A. Bjurlin and R. S. Matulewicz, *Comprehensive Diagnostic Approach to Bladder Cancer, Molecular Imaging and Biomarkers*, 2021.
- 88 M. Sitara, W. Zhang, H. Gao, J. Li and J. Tian, *Chem. Biomed. Imaging*, 2024, **2**, 526–541.
- 89 V. S. Vaidya, J. S. Ozer, F. Dieterle, F. B. Collings, V. Ramirez, S. Troth, N. Muniappa, D. Thudium, D. Gerhold, D. J. Holder, N. A. Bobadilla, E. Marrer, E. Perentes, A. Cordier, J. Vonderscher, G. Maurer, P. L. Goering, F. D. Sistare and J. V. Bonventre, *Nat. Biotechnol.*, 2010, **28**, 478–485.
- 90 E. E. Mulvihill and D. J. Drucker, *Endocr. Rev.*, 2014, **35**, 992–1019.
- 91 J. H. Suh and J. H. Miner, *Nat. Rev. Nephrol.*, 2013, **9**, 470–477.
- 92 R. E. Baker, A. S. Mahmud, I. F. Miller, M. Rajeev, F. Rasambainarivo, B. L. Rice, S. Takahashi, A. J. Tatem, C. E. Wagner, L. F. Wang, A. Wesolowski and C. J. E. Metcalf, *Nat. Rev. Microbiol.*, 2022, **20**, 193–205.
- 93 A. M. Caliendo, D. N. Gilbert, C. C. Ginocchio, K. E. Hanson, L. May and T. C. Quinn, *Clin. Infect. Dis.*, 2014, **58**, 1346.
- 94 W. O. C. M. Cookson, M. J. Cox and M. F. Moffatt, *Nat. Rev. Microbiol.*, 2018, **16**, 111–120.
- 95 J. B. Humbwavali, N. J. Trujillo, B. S. Paim, F. H. Wolff and N. T. Barcellos, *Lancet Infect. Dis.*, 2011, **11**, 160.
- 96 V. Dartois and T. Dick, *Nat. Rev. Drug Discovery*, 2024, **23**, 381–403.
- 97 D. L. Goldenberg, *Lancet*, 1998, **351**, 197–202.
- 98 H. K. Kwon, I. Lee, K. E. Yu, S. V. Cahill, K. D. Alder, S. Lee, C. M. Dussik, J. Back, J. Choi, L. Song, T. R. Kyriakides and F. Y. Lee, *Sci. Adv.*, 2021, **7**, eabf2665.



- 99 E. Y. H. Xin, G. Kwek, X. An, C. Sun, S. Liu, N. S. Qing, S. Lingesh, L. Jiang, G. Liu and B. Xing, *Angew. Chem., Int. Ed.*, 2024, **63**, e202406843.
- 100 W. C. Albrich, C. R. Kahlert, S. Nigg, L. F. Boesel and G. Giovannini, *Anal. Chem.*, 2024, **96**, 20578–20586.
- 101 L. Mendive-Tapia, D. Mendive-Tapia, C. Zhao, D. Gordon, S. Benson, M. J. Bromley, W. Wang, J. Wu, A. Kopp, L. Ackermann and M. Vendrell, *Angew. Chem., Int. Ed.*, 2022, **61**, e202117218.
- 102 Y. C. Wang, Y. T. Huang, R. C. Chase, T. Li, D. Ramai, S. Li, X. Q. Huang, S. O. Antwi, A. P. Keaveny and M. Y. Pang, *Gastroenterology*, 2023, **165**, 773–783.
- 103 S. D. Melton, R. M. Genta and R. F. Souza, *Nat. Rev. Gastroenterol. Hepatol.*, 2010, **7**, 620–628.
- 104 M. S. Petrov and D. Yadav, *Nat. Rev. Gastroenterol. Hepatol.*, 2019, **16**, 175–184.
- 105 C. Wüster, H. Y. Shi, C. M. Kühlbrey, E. A. Biesel, U. T. Hopt, S. Fichtner-Feigl and U. A. Wittel, *Ann. Surg.*, 2020, **272**, 863–870.
- 106 A. Henderson, *Lancet*, 1996, **348**, s1–s4.
- 107 L. Wu, Y. Ishigaki, Y. Hu, K. Sugimoto, W. Zeng, T. Harimoto, Y. Sun, J. He, T. Suzuki, X. Jiang, H. Y. Chen and D. Ye, *Nat. Commun.*, 2020, **11**, 446.
- 108 D. J. Polhemus and D. J. Lefer, *Circ. Res.*, 2014, **114**, 730–737.
- 109 A. Y. Y. Cheng, M. B. Gomes, S. Kalra, A. P. Kengne, C. Mathieu and J. E. Shaw, *Nat. Rev. Endocrinol.*, 2023, **19**, 194–200.
- 110 M. Casciaro, E. Di Salvo, E. Pace, E. Ventura-Spagnolo, M. Navarra and S. Gangemi, *Immun. Ageing*, 2017, **14**, 21.
- 111 D. Rutkowski, R. Scholey, J. Davies, D. Pye, F. Blackhall, R. B. Warren, F. Jimenez, C. E. M. Griffiths and R. Paus, *Br. J. Dermatol.*, 2024, **191**, 791–804.
- 112 D. Choi, O. Waksman, A. Shaik, P. Mar, Q. Z. Chen, D. J. Cho, H. Kim, R. L. Smith, S. N. Goonewardena and R. S. Rosenson, *J. Am. Coll. Cardiol.*, 2022, **80**, 316–328.
- 113 M. X. Liang, Q. Wang, S. Zhang, Q. Lan, R. J. Wang, E. C. Tan, L. Zhou, C. P. Wang, H. Wang and Y. Y. Cheng, *Adv. Mater.*, 2024, **36**, 2409015.
- 114 L. Zhu and W. Lin, *Sens. Actuators, B*, 2022, **352**, 131042.
- 115 S. K. Nandi, D. Singh, J. Upadhyay, N. Gupta, N. Dhiman, S. K. Mittal and N. Mahindroo, *Int. J. Biol. Macromol.*, 2021, **193**, 838–846.
- 116 A. Lleó, E. Cavedo, L. Parnetti, H. Vanderstichele, S. K. Herukka, N. Andreasen, R. Ghidoni, P. Lewczuk, A. Jeromin, B. Winblad, M. Tsolaki, B. Mroczko, P. J. Visser, I. Santana, P. Svenningsson, K. Blennow, D. Aarsland, J. L. Molinuevo, H. Zetterberg and B. Mollenhauer, *Nat. Rev. Neurol.*, 2015, **11**, 41–55.
- 117 C. L. Masters, R. Bateman, K. Blennow, C. C. Rowe, R. A. Sperling and J. L. Cummings, *Nat. Rev. Dis. Primers*, 2015, **1**, 15059.

